© 2021. Published by The Company of Biologists Ltd | Development (2021) 148, dev194787. doi:10.1242/dev.194787

STEM CELLS AND REGENERATION

RESEARCH ARTICLE

Oxygen regulates epithelial stem cell proliferation via RhoA-actomyosin-YAP/TAZ signal in mouse incisor

Keishi Otsu[1], Hiroko Ida-Yonemochi[2], Shojiro Ikezaki[1], Masatsugu Ema[3], Jiro Hitomi[4], Hayato Ohshima[2] and Hidemitsu Harada[1,*]

ABSTRACT

Stem cells are maintained in specific niches that strictly regulate their proliferation and differentiation for proper tissue regeneration and renewal. Molecular oxygen (O_2) is an important component of the niche microenvironment, but little is known about how O_2 governs epithelial stem cell (ESC) behavior. Here, we demonstrate that O_2 plays a crucial role in regulating the proliferation of ESCs using the continuously growing mouse incisors. We have revealed that slow-cycling cells in the niche are maintained under relatively hypoxic conditions compared with actively proliferating cells, based on the blood vessel distribution and metabolic status. Mechanistically, we have demonstrated that, during hypoxia, HIF1α upregulation activates the RhoA signal, thereby promoting cortical actomyosin and stabilizing the adherens junction complex, including merlin. This leads to the cytoplasmic retention of YAP/TAZ to attenuate cell proliferation. These results shed light on the biological significance of blood-vessel geometry and the signaling mechanism through microenvironmental O_2 to orchestrate ESC behavior, providing a novel molecular basis for the microenvironmental O_2-mediated stem cell regulation during tissue development and renewal.

KEY WORDS: Epithelial stem cells, Oxygen, RhoA, YAP/TAZ, Actomyosin, Rodent incisor

INTRODUCTION

Stem cells (SCs) possess the ability of self-renewal and differentiation into specialized cell types. This characteristic is essential to create new tissues and organs during development and to maintain tissue homeostasis (Wabik and Jones, 2015). SC proliferation is controlled by intrinsic (cell-autonomous) and extrinsic (environmental) cues, and collapse of the regulation causes serious events (Chen et al., 2012; Pietras et al., 2011). Thus, understanding the mechanisms governing SC proliferation is crucial.

In ectodermal appendages that undergo continuous cell turnover, such as teeth, hair follicles, mammary glands and nails, epithelial stem cells (ESCs) reside in a niche, a physiologically limited microenvironment, containing a heterogeneous cell population with different proliferation rates, such as slow-cycling cells (SCCs) and actively dividing transit-amplifying cells (TACs) (Harada et al., 1999; Hsu et al., 2014; Wabik and Jones, 2015).

In particular, the rodent incisor, which grows continuously throughout the life of the animal, provides an excellent model to investigate the characteristics and regulation of SCs in general, because teeth share many developmental mechanisms with other ectodermal organs. To counterbalance constant abrasion, the self-renewal of the dental epithelium located on the labial side covered with enamel is supported by the continuous supply of cells at the proximal end, called the apical bud (Harada et al., 1999) (Fig. 1A,B). Previously, it has been proposed that the incisors follow a classical SC paradigm. A few SCCs reside in the outer enamel epithelium (OEE) and the stellate reticulum (SR) as dental epithelial stem cells (DESCs). They asymmetrically divide to give rise to TACs in the inner enamel epithelium (IEE) through the basal epithelium (BE). Then, the IEE moves distally, ceases proliferation and undergoes differentiation into ameloblasts to form the enamel (Harada et al., 1999; Kuang-Hsien Hu et al., 2014) (Fig. 1C,D). This model is based on the lineage tracing of putative SC markers (Juuri et al., 2012; Seidel et al., 2017). Recently, it has been proposed that TACs in IEE undergo self-renewal and contribute to the formation of both SCCs and ameloblasts following single-cell RNA-sequencing studies and advanced computational techniques (Sharir et al., 2019). Thus, although the identity, hierarchies and kinetic of the DESCs are still under investigation, cell proliferation in the niche must be tightly regulated for proper development and renewal. To date, a number of signaling pathways regulating DESCs have been studied (Yu and Klein, 2020). However, the impact of niche microenvironment on their dynamics remains poorly understood.

Molecular oxygen (O_2) is involved in a wide range of cellular functions and metabolism. Recently, increasing evidence indicates that O_2 as a niche component plays an essential role in the maintenance of stem cells and in cell fate decisions. For example, in hematopoietic SCs residing in the sinusoidal hypoxic area distant from the blood vessels, hypoxia maintains their undifferentiated state and influences their proliferation and cell-fate commitment (Kubota et al., 2008). The hypoxic response is mediated by hypoxia-inducible transcription factors (HIFs) that are stabilized under hypoxia and regulate gene expression (Takubo et al., 2010) and intracellular signaling pathways (Choi et al., 2017; Gustafsson et al., 2005). In contrast, high O_2 concentration accelerates cellular aging, which leads to the loss of SC properties (Csete, 2005). These signaling cascades and transcriptional programs induced by O_2 appear to be shared by many SCs (Lin et al., 2008; Mohyeldin et al., 2010; Simon and Keith, 2008). However, in epithelial tissues, although the regulatory mechanism of SCs have been gradually elucidated (Morrison and Spradling, 2008), no comprehensive data on how O_2 is involved in the regulation of SC proliferation are available.

[1]Division of Developmental Biology and Regenerative Medicine, Department of Anatomy, Iwate Medical University, 1-1-1, Idaidori, Yahaba, Iwate 028-3694, Japan. [2]Division of Anatomy and Cell Biology of the Hard Tissue, Department of Tissue Regeneration and Reconstruction, Niigata University Graduate School of Medical and Dental Sciences, 2-5274 Gakkocho-dori, Chuo-ku, Niigata 951-8514, Japan. [3]Department of Stem Cells and Human Disease Models, Research Center for Animal Life Science, Shiga University of Medical Science, Shiga 520-2192, Japan. [4]Division of Human Embryology, Department of Anatomy, Iwate Medical University, 1-1-1, Idaidori, Yahaba, Iwate 028-3694, Japan.

*Author for correspondence (hideha@iwate-med.ac.jp)

H.O., 0000-0001-8571-9900; H.H., 0000-0002-9724-8568

Handling Editor: Patrick Tam
Received 8 July 2020; Accepted 11 January 2021

Development (2021) 148, dev194787. doi:10.1242/dev.194787

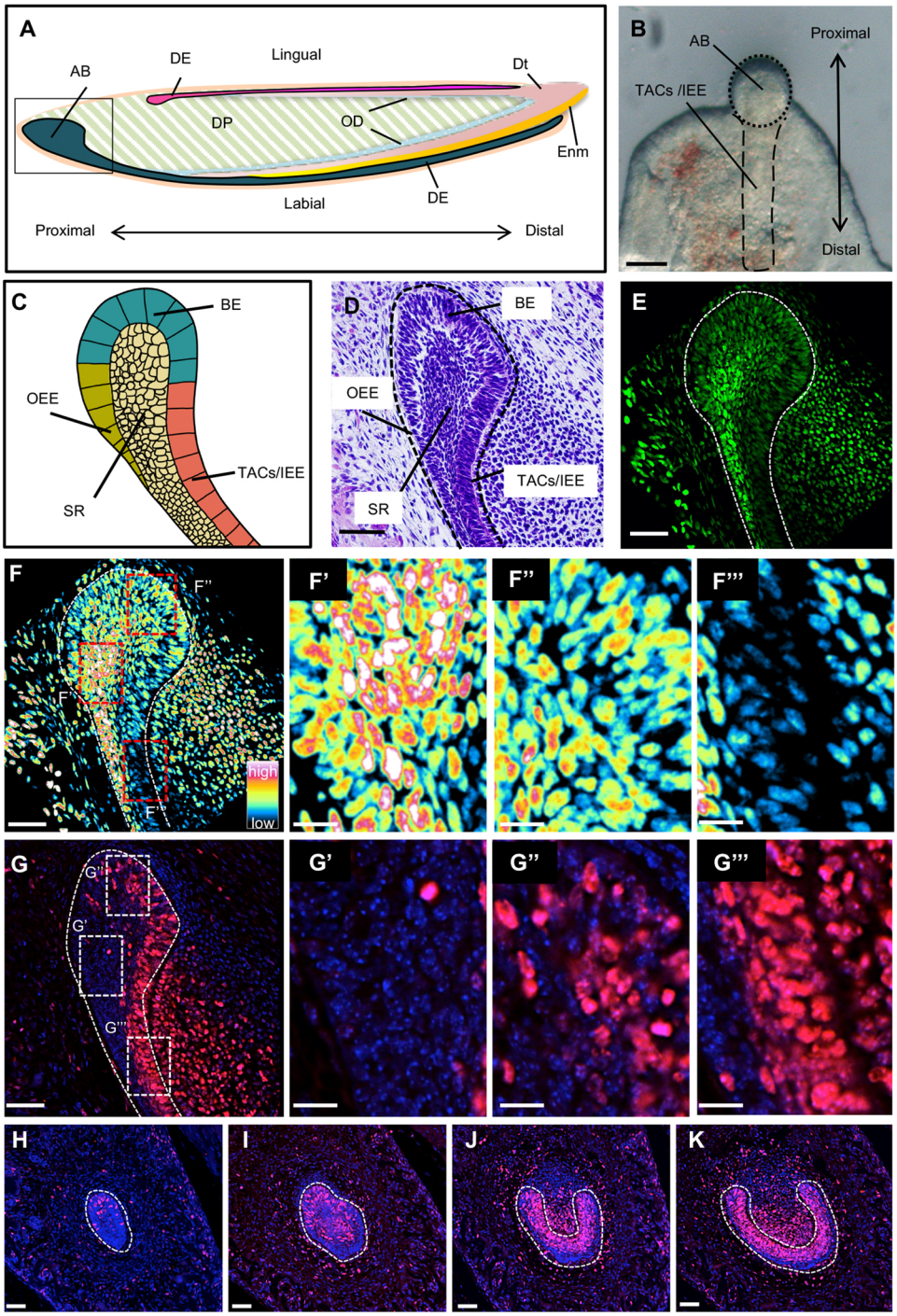

Fig. 1. Cell proliferation profile of the apical bud. (A) Schematic showing sagittal views of a mouse lower incisor. (B) Stereo front view of the epithelium of the proximal end of a P3 mouse incisor. (C) Schematic showing magnified sagittal section of an apical bud. (D) H&E staining of the sagittal section of an apical bud. (E) GFP image of an apical bud of H2B-GFP mice at the indicated time after pulse treatment with Dox. Dashed line delimits the dental epithelium. (F-F‴) The pseudo-color images in F show the relative intensity of GFP fluorescence. Pixel intensity values ranged from 0 (black) to 255 (white) as illustrated by the color-scale bar. The magnifications of the areas indicated by the red dashed boxes are shown on the right. (G-G‴) Ki67 immunostaining of the apical bud of a P3 WT mouse incisor. Magnifications of the areas indicated by white dashed boxes are shown on the right. In merged images, the nucleus is stained with DAPI (blue). (H-K) Ki67 immunostaining of the serial frontal section from the proximal end to the distal end of a WT P3 mouse incisor. AB, apical bud; BE, basal epithelium; DE, dental epithelium; DP, dental pulp; Dt, dentin; Enm, enamel; IEE, inner enamel epithelium; OD, odontoblasts; OEE, outer enamel epithelium; SR, stellate reticulum; TACs, transit amplifying cells. Scale bars: 100 µm (B); 50 µm (D,E,F,G,H-K); 10 µm (F′-F‴,G′-G‴).

RhoA, the founding member of the Rho family GTPase, influences many biological processes, including cell cycle progression and proliferation (Coleman et al., 2004). RhoA is a molecular switch that cycles between inactive GDP-bound and active GTP-bound forms. The GTP-bound active RhoA associates with the downstream effector protein Rho-associated protein kinase (ROCK), which promotes the polymerization and stabilization of filamentous actin (F-actin), the phosphorylation of myosin light chain (MLC) and myosin ATPase activity, leading to actomyosin tension (Jaffe and Hall, 2005; Ridley, 1996; Riento and Ridley, 2003). Actomyosin in non-muscle cells controls cell shape and motility and functions as a mechanical stressor. Recently, we have demonstrated that RhoA signal regulates the cell proliferation of dental epithelial cells via the reorganization of actomyosin and the adherens junction (AJ) (Otsu et al., 2016, 2011), indicating that the RhoA signal is a potent regulator of cell proliferation of DESCs. However, its upstream and downstream components have yet to be identified.

Yes-associated protein (YAP) and its homolog, the transcriptional co-activator with PDZ binding motif (TAZ), are transcriptional cofactors that shuttle between the cytoplasm and nucleus and can be dependent on the Hippo pathway (Lei et al., 2008; Zhao et al., 2007). In the nucleus, YAP/TAZ associate with several promoters of specific transcription factors, which activate

Development (2021) 148, dev194787. doi:10.1242/dev.194787

genes regulating cell proliferation for the control of organ size in both *Drosophila* and mammals (Dong et al., 2007). YAP/TAZ are also involved in cell-fate decisions as a stemness factor in different SC pools of the body (Camargo et al., 2007; Watt et al., 2010). In several tissues, YAP/TAZ regulate the proliferation and differentiation of stem/progenitor cells (Cao et al., 2008; Hu et al., 2017; Schlegelmilch et al., 2011). Recently, in rodent incisors, YAP/TAZ have been reported to control the proliferation and differentiation of TACs in response to integrin/FAK signaling (Hu et al., 2017). Further, the activity of YAP/TAZ has recently been linked to mechanical and cytoskeletal signals. Previous studies have shown that cortical actomyosin and stress fibers are involved in nuclear translocation of YAP/TAZ (Furukawa et al., 2017; Wada et al., 2011).

In this study, we explore the role of microenvironmental O_2 in ESCs and its molecular regulatory mechanism using the mouse incisor model. We hypothesized that RhoA-mediated actomyosin regulates YAP/TAZ activity to control the cell proliferation of DESCs. We found that microenvironmental O_2 is an important regulator of SC proliferation through the RhoA-actomyosin-YAP/TAZ signal. Our study offers a conceptual framework in understanding environment-mediated SC regulation, thus aiding in the development of SC-based regeneration therapy.

RESULTS

Cell proliferation profile of the apical bud

We first visualized the cell proliferation profile of the apical bud in the tetracycline-regulatable Histone 2B-Green Fluorescent Protein (H2B-GFP) transgenic mouse incisor model, in which the fusion protein of H2B-GFP is expressed after doxycycline (DOX) administration. GFP fluorescence was diluted twofold at each division, therefore it is retained preferentially in slowly dividing cells. In the lower incisor of postnatal day (P) 3 mouse after one DOX administration at embryonic day (E) 16.5, the GFP label retaining SCCs was found in the OEE and outside SR, whereas GFP was gradually decreased from the inside of SR to IEE through BE (Fig. 1E,F). Consistent with this observation, the number of Ki67-positive proliferating cells increased from the apical bud to TACs in P3 wild-type (WT) mice (Fig. 1G-K; Fig. S1A).

SCCs are maintained under hypoxia compared with TACs

To estimate the oxygen concentration in tissues around the apical bud, we analyzed the blood vessel distribution. Stereomicroscopic images of the mouse incisor immediately after extraction showed that few blood vessels are visible around the apical bud (Fig. 2A,B, asterisk). To investigate the distribution of blood vessels inside the incisor, we analyzed the tissue sections of transgenic FLK1-GFP mice with GFP and the FLK1 (VEGFR-2; also known as Kdr) promoter. In both the frontal and sagittal sections, the apical bud was at a distance from the blood vessels (Fig. 2C-E), whereas the high-density blood vessels were close to highly proliferating TACs and pre-odontoblasts/odontoblasts (Fig. 2C,F, arrowheads). Further, HIF1α was strongly expressed in SCCs in the apical bud compared with TACs (Fig. 2G; Fig. S1B). These results suggest that more oxygen was supplied to TACs than to SCCs.

We further examined the difference of the metabolic program between SCCs and TACs. The expression of pyruvate dehydrogenase (PDH), which aerobically catalyzes the conversion of pyruvate to acetyl-CoA for use in mitochondrial metabolism (Harris et al., 2002), and of citrate synthase, the first and rate-limiting enzyme of the tricarboxylic acid (TCA) cycle for oxidative phosphorylation (OXPHOS) in mitochondria (Cheng et al., 2009), was higher in TACs than in SCCs (Fig. 2H,I). Moreover, scanning electron microscopy (SEM) revealed that the shape of mitochondria in H2B-GFP-positive SCCs was spherical, whereas that in GFP-negative TACs was tubular. The size of mitochondria in SCCs was smaller than that in TACs (Fig. 2J-M). These results indicate that SCCs preferentially use anaerobic glycolysis, whereas TACs undergo a metabolic switch towards OXPHOS to meet the cell energy demand for proliferation, thereby requiring more oxygen consumption and mitochondrial biogenesis. Taken together, these results strongly suggest that SCCs are maintained in a relatively hypoxic environment compared with TACs, dependent on the distance from blood vessels.

Hypoxia restrained cellular proliferation and YAP/TAZ expression in the apical bud

To ascertain whether cell proliferation in the apical bud is dependent on environmental O_2 concentration, we cultured mouse incisors under hypoxic condition. Stereomicroscopic images showed that, in hypoxia (5% O_2), the length of the dental epithelium was shorter and the area of the apical bud was smaller than in normoxia (21% O_2) (Fig. 3A-C). Consistent with the suppression of epithelial growth, the number of Ki67-positive cells was reduced by hypoxia in the apical bud (Fig. 3D,E; Fig. S2A) without inducing apoptosis (Fig. S3A). Then, we evaluated the association between environmental O_2 and YAP/TAZ expression and confirmed the strong immunoreaction of the antibodies against YAP/TAZ and YAP1 in TACs (Fig. 3F, arrows; Fig. S1C,D), whereas TAZ was predominantly expressed in the cytosol and showed no significant differences between TACs and the apical bud (Fig. 3G; Fig. S1E). The organ culture of mouse incisors showed that hypoxia reduced the number of nuclear YAP/TAZ- and YAP1-positive cells (Fig. 3H,I; Fig. S2B).

In addition, we investigated the effect of O_2 concentration on cell proliferation and the expression of YAP/TAZ in mHAT9d cells, originally established from the apical bud of a mouse incisor (Harada and Ohshima, 2004; Harada and Otsu, 2019; Kawano et al., 2002). Previous studies have reported that cell proliferation and YAP/TAZ expression in cultured epithelial cells were dependent on cell density (Zhao et al., 2007). In normoxia, low-density mHAT9d cells were actively proliferated, whereas Ki67, YAP/TAZ and YAP1 were strongly expressed in the nucleus (Fig. S4). In contrast, high-density mHAT9d cells were negative for Ki67, whereas YAP/TAZ and YAP1 were present in the cytosol (Fig. S4). We also demonstrated that the knockdown of YAP1 using small interfering RNA (siRNA) reduced cell proliferation of low-density mHAT9d cells, confirming YAP1 involvement in cell proliferation (Fig. S5).

Low-density mHAT9d cell culture under hypoxic conditions showed that cell proliferation and nuclear YAP/TAZ and YPA1 expression were significantly decreased compared with those under normoxic conditions, without inducing apoptosis (Figs S3B and S6A-F). Hypoxia also decreased the YAP1 mRNA expression, but not TAZ (Fig. S6G). Together, these results were consistent with the hypothesis that hypoxia repressed cell proliferation through the inhibition of YAP/TAZ activity in the apical bud.

Hypoxia-activated RhoA signaling

We have previously demonstrated that the downregulation of RhoA/ROCK signal promotes cellular proliferation in the apical bud (Otsu et al., 2016, 2011). Thus, we hypothesized that the oxygen- and

Development (2021) 148, dev194787. doi:10.1242/dev.194787

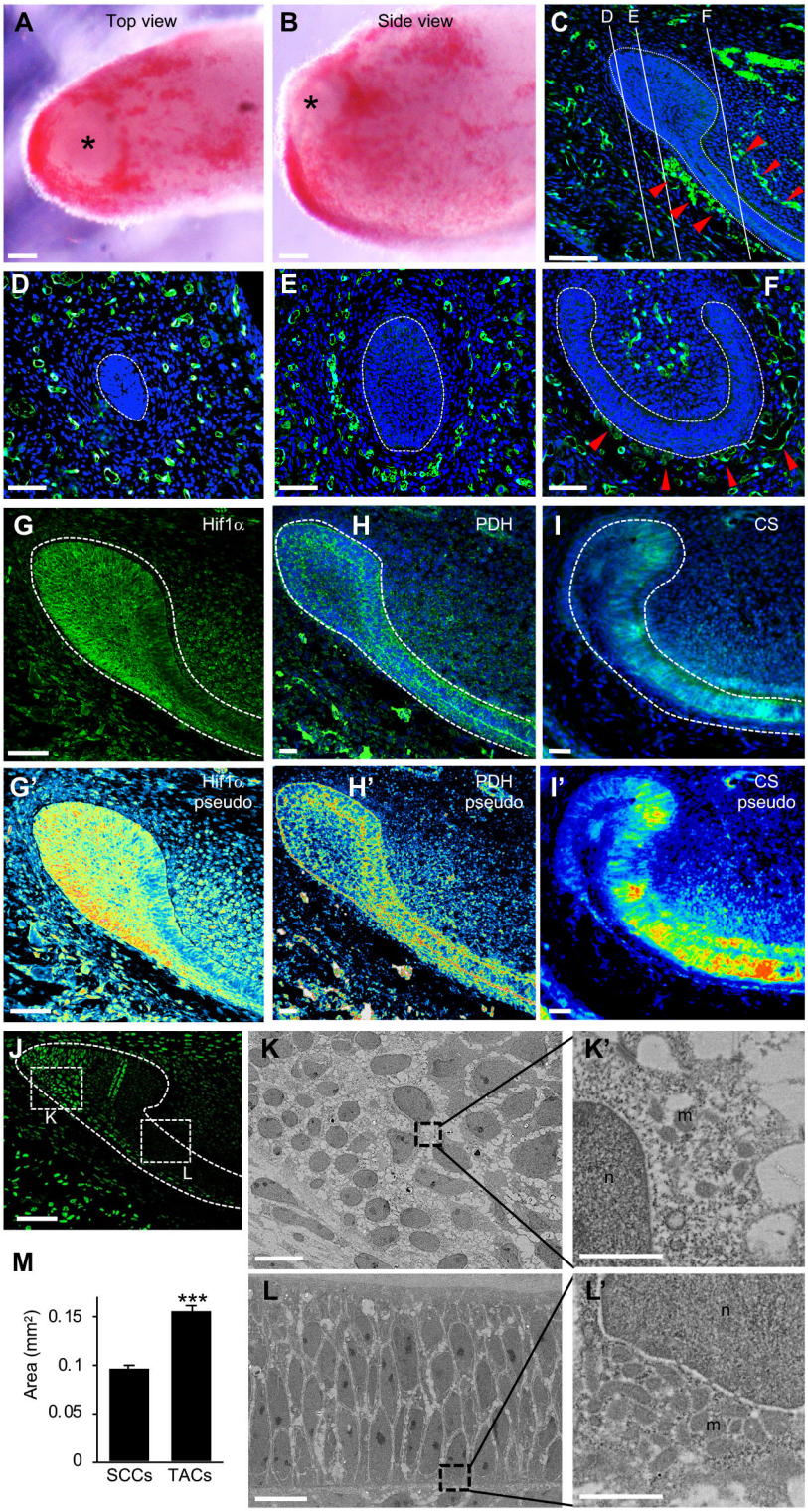

Fig. 2. SCCs are maintained under hypoxia compared with TACs. (A,B) Stereomicroscope images of a P3 mouse lower incisor immediately after extraction. Top view (A) and side view (B). Asterisk indicates the apical bud. (C-F) Fluorescent images of the sagittal (C) and frontal sections (D-F) of P3 FLK1-GFP mouse lower incisor. Lines in C indicate the position of the serial frontal sections in D-F. The arrowheads indicate dense blood vessels close to the dental epithelium. Dashed line delimits the dental epithelium. (G-I′) HIF1α (G,G′), pyruvate dehydrogenase (PDH; H,H′) and citrate synthase (CS; I,I′) immunostaining of the apical bud in P3 WT mice lower incisors. G′,H′,I′ show pseudo-color images indicating the relative intensity of HIF1α, PDH, CS fluorescence. (J-L′) Comparison of mitochondrial morphology between SCCs and TACs using array tomography. Fluorescent images of the apical bud in a P3 H2B-GFP mouse lower incisor (J). The area surrounded by the dotted line is observed through SEM. SEM images of GFP-retaining SCCs (K,K′) and GFP-negative TACs (L,L′). (M) The quantification of the average area of mitochondria in SCCs and TACs; n=224 mitochondria. Data are mean±s.e.m. ***P<0.001 (unpaired two-tailed Student's t-test). n, nucleus; m, mitochondria. Scale bars: (A,B,C) 100 µm; (D-F) 50 µm; (G-I,G′-I′,J) 20 µm; (K,L) 10 µm; (K′,L′) 1.5 µm.

YAP/TAZ-dependent cell proliferation is mediated by RhoA signaling. Immunohistochemistry illustrated that the expression of active RhoA (GTP-binding form), phosphorylated myosin light chain (pMLC) and F-actin, a downstream event of RhoA, was higher in SCCs in the apical bud than in TACs (Fig. 4A,B; Fig. S1F-H). These indicated that RhoA signaling is more active in SCCs under hypoxic conditions *in vivo*. To determine whether the activity of RhoA in dental epithelial cells is dependent on environmental O_2 concentration, we cultured mouse incisors under hypoxic conditions and showed that hypoxia increased the expression of active RhoA, HIF1α, F-actin and pMLC in dental epithelium (Fig. 4C; Fig. S2C-E). Similarly, we have observed that hypoxia also increased active RhoA and HIF1α expressions in mHAT9d cells (Fig. 4D,E,H,J). Further, HIF1α knockdown decreased active RhoA expression during hypoxia in mHAT9d cells (Fig. 4E-G,I,J), indicating that HIF1α mediated hypoxia-induced RhoA activation.

Development (2021) 148, dev194787. doi:10.1242/dev.194787

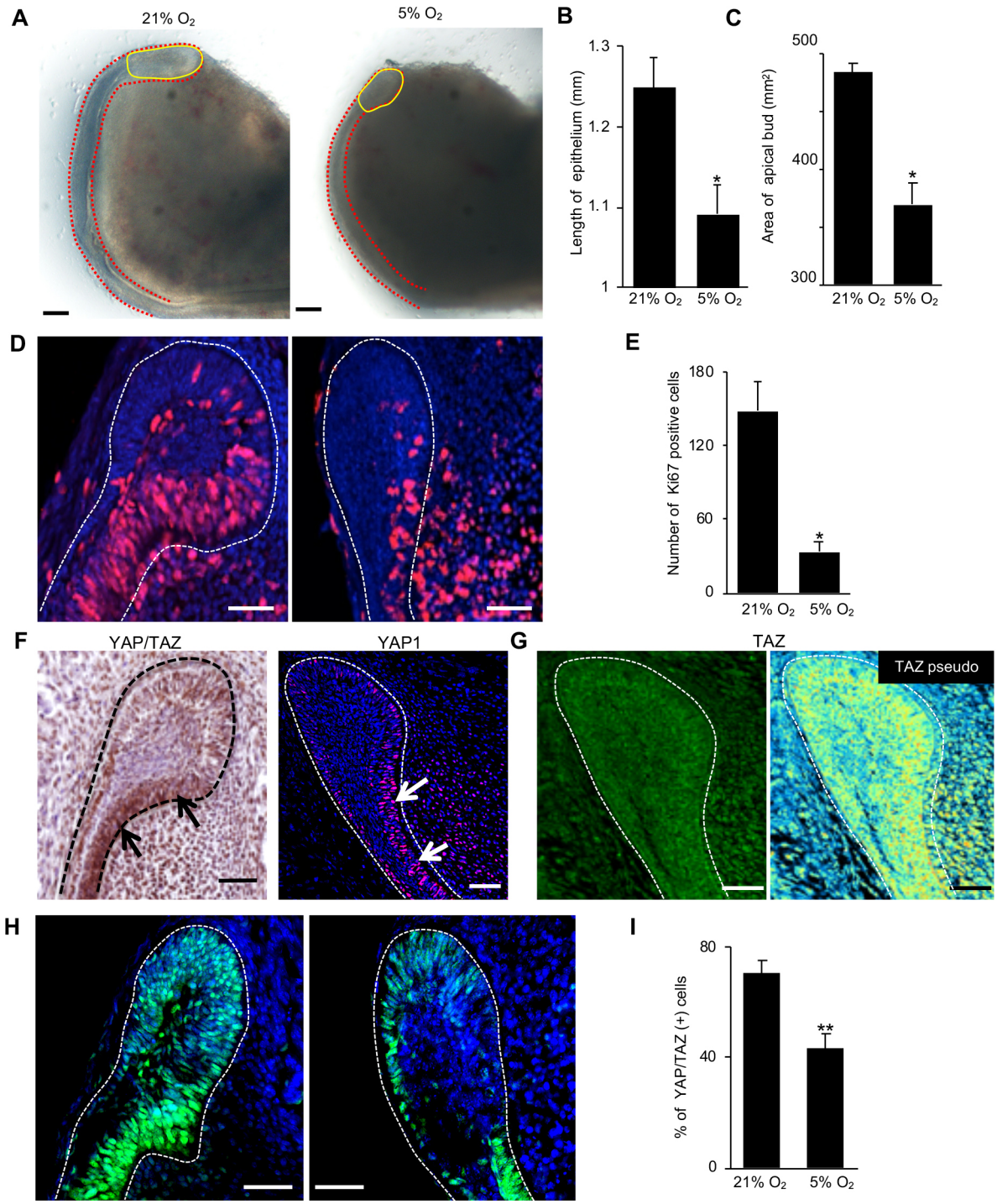

Fig. 3. Hypoxia restrained cellular proliferation and YAP/TAZ in the apical bud. (A) Stereomicroscopic images of the apical end of a mouse lower incisor cultured in normoxia (21% O_2; left) and hypoxia (5% O_2; right) for 2 days. The dashed red line delimits the dental epithelium. Areas surrounded by yellow lines indicate the apical bud. (B,C) The average length of the epithelium (B) and the area of the apical bud (C) are quantified; *n*=6. (D) Ki67 staining (magenta) of the apical bud cultured in normoxia (left) and hypoxia (right). (E) The number of Ki67-positive cells in the apical bud was quantified; *n*=4. (F) Immunostaining of YAP/TAZ (left) and YAP1 (right) in the apical bud of a P2 mouse lower incisor. Arrows indicate the strong immunoreaction of the antibodies against YAP/TAZ and YAP1. (G) Immunostaining of TAZ in the apical bud of a P2 mouse lower incisor. Pseudo-color image (right) shows the relative intensity of TAZ fluorescence. (H) Immunostaining of YAP/TAZ (green) in the apical bud cultured in normoxia (left) and hypoxia (right) for 2 days. (I) The percentage of YAP/TAZ-positive (+) cells per section is quantified; *n*=4. Data are mean±s.e.m. **P*<0.05, ***P*<0.01 (unpaired two-tailed Student's *t*-test). Scale bars: 100 µm (A); 30 µm (D,H); 50 µm (F,G).

RhoA/ROCK signaling is required for maintenance of cortical actomyosin and AJ

We examined the detailed role of the RhoA/ROCK signal on actomyosin in mHAT9d cells. High-density mHAT9d cells exhibited a distinct cortical expression of F-actin and pMLC compared with low-density cells (Fig. S7). However, Y27632, an inhibitor of RhoA/ROCK-mediated actomyosin, diminished this distinct expression, induced a morphological change from cuboidal

Development (2021) 148, dev194787. doi:10.1242/dev.194787

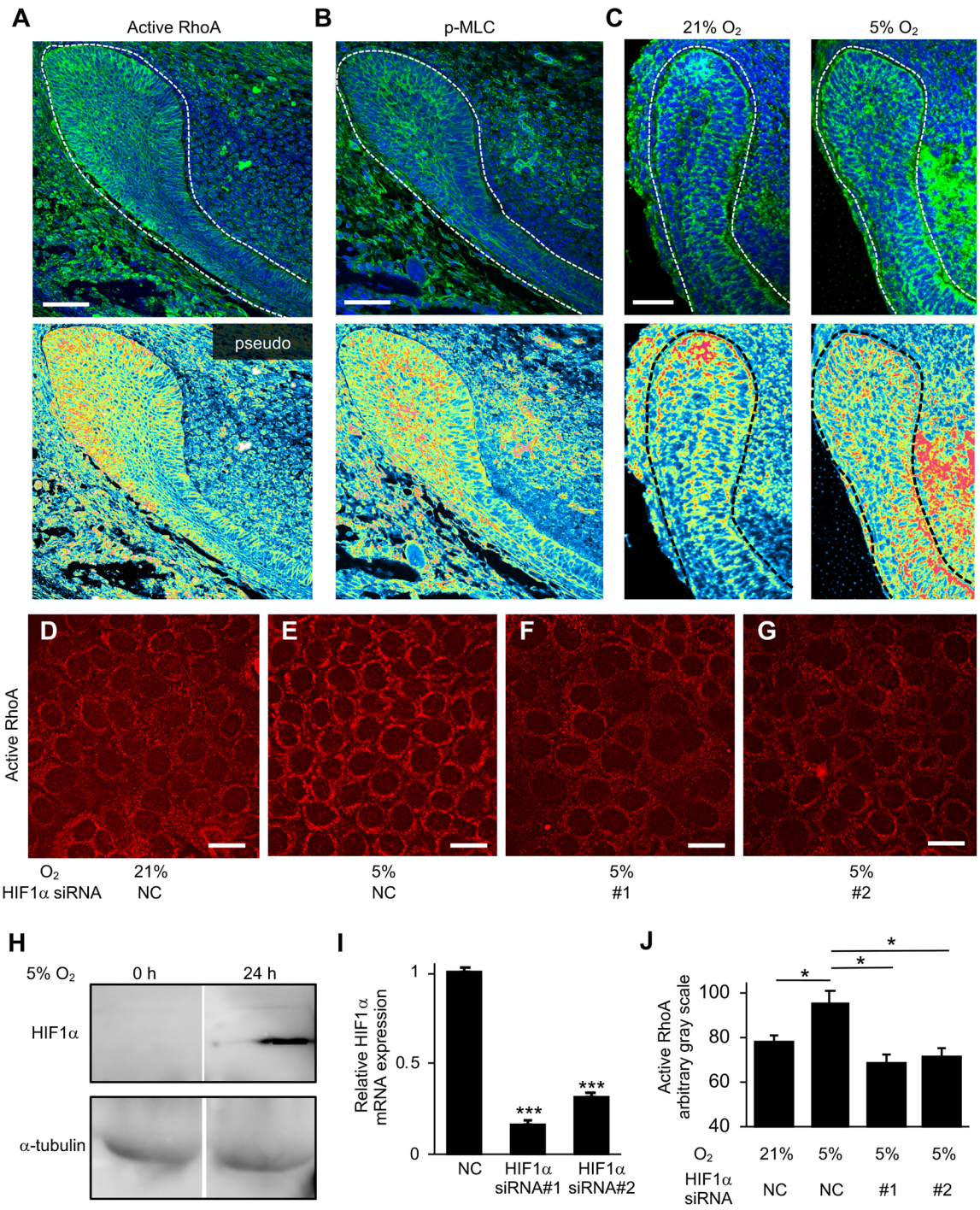

Fig. 4. Hypoxia activated RhoA signaling. (A,B) Immunostaining for Active RhoA (A) and p-MLC (B) in the apical bud of WT P3 mouse lower incisors. (C) Active RhoA expression in the apical bud cultured in normoxia (left) and hypoxia (right) for 2 days. Pseudo-color images (bottom) show the relative intensity of active RhoA and p-MLC fluorescence. (D-G) Immunofluorescence of active RhoA in mHAT9d cells transfected with non-specific control siRNA (NC) or two different siRNA specific for HIF1α in normoxia and hypoxia. (H) Immunoblotting for HIF1α and α-tubulin in mHAT9d cells cultured in hypoxia for 0 h and 24 h. (I) Expression of HIF1α mRNA in mHAT9d cells transfected with non-specific control siRNA (NC) or siRNA specific for HIF1α in hypoxia; n=3. (J) Quantification of active RhoA fluorescence in D-G; n=4. Data are mean±s.e.m. *P<0.05, ***P<0.001 (unpaired two-tailed Student's t-test). Scale bars: 50 µm (A-C); 20 µm (D-G).

into spindle-shaped, and enlarged cell size (Fig. 5A,B), suggesting a decrease in the cortical tension in cells. Similarly, blebbistatin, a selective myosin II ATPase inhibitor, caused a reduction in cortical actomyosin and a morphological change (Fig. 5A,B).

Because cortical actomyosin is connected to the AJ and maintains its structure and function in epithelial cells (Lecuit and Yap, 2015), we next investigated the involvement of RhoA/ROCK-mediated actomyosin in AJ. AJ proteins, such as E-cadherin (E-cad), α-catenin, β-catenin and merlin (Nf2), were co-expressed at the cell periphery (Fig. S8), whereas Y27632 and blebbistatin diminished their expression in mHAT9d cells (Fig. 5C). Y27632 also decreased E-cad expression in the apical bud of the cultured

Development (2021) 148, dev194787. doi:10.1242/dev.194787

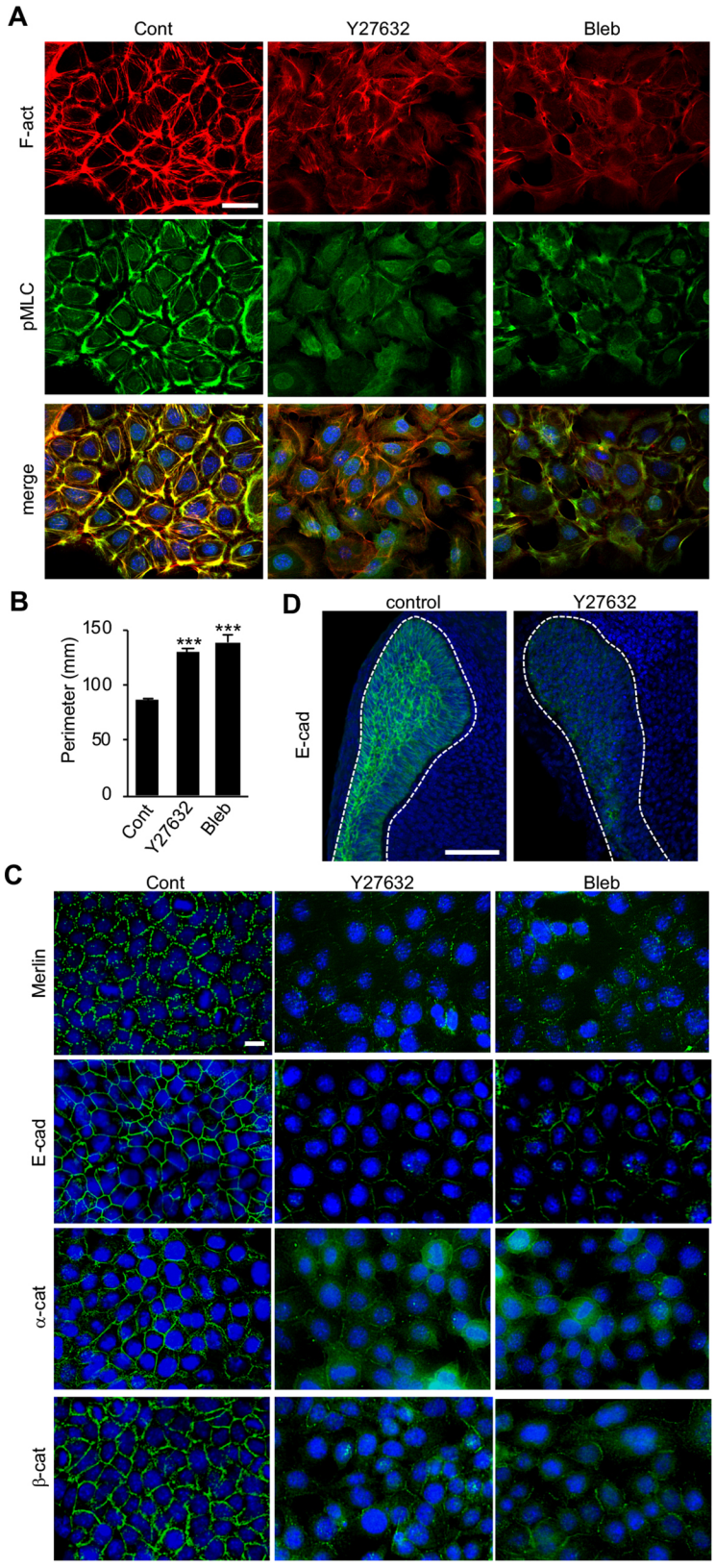

Fig. 5. RhoA/ROCK signaling is required for the maintenance of cortical actomyosin and adherens junctions. (A) Phalloidin staining (F-actin) and immunostaining for pMLC of high-density mHAT9d cells after treatment with vehicle (cont), Y27632 or blebbistatin (Bleb) for 24 h. (B) Quantification of the average perimeter of the cells; n=4. Data are mean±s.e.m. ***P<0.001 (unpaired two-tailed Student's t-test). (C) Immunostaining for Merlin, E-cadherin (E-cad), α-catenin (α-cat) and β-catenin (β-cat) of high-density mHAT9d cells after treatment with Y27632 and Bleb for 24 h. (D) Immunostaining for E-cad in the apical bud after treatment with Y27632 for 3 days. Scale bars: 30 µm (A); 20 µm (C); 50 µm (D).

mouse incisors (Fig. 5D). In addition, we have confirmed that E-cad and merlin are weakly expressed in TACs compared with the apical bud *in vivo* (Figs S1I,J and S9A, arrows), which coincided with the RhoA activation status (Fig. 4). Furthermore, in cultured incisors and mHAT9d cells, hypoxia increased expression of E-cad and merlin (Figs S2F,G and S9B,C), whereas HIF1α knockdown enlarged cell size and reduced the peripheral expression of E-cad, merlin and F-actin (Fig. S9D,E). Together, these results indicate that

Development (2021) 148, dev194787. doi:10.1242/dev.194787

the hypoxia-RhoA signal is involved in the maintenance of cortical actomyosin and the AJ.

RhoA/ROCK-mediated cortical actomyosin regulates YAP/TAZ and cell proliferation

We also investigated whether the RhoA-mediated cortical actomyosin regulates cell proliferation and YAP/TAZ localization. Y27632 and blebbistatin increased cell proliferation (Fig. 6A) and induced the nuclear translocation of YAP/TAZ in high-density mHAT9d cells (Fig. 6B). Similarly, in cultured mouse incisor, Y27632 increased YAP/TAZ expression in the apical bud (Fig. 6C). Y27632 and blebbistatin reduced the cytosolic expression of phosphorylated YAP (pYAP; S127) and phosphorylated LATS1/2 (pLATS1/2) (Fig. 6D,E), both of which are essential for the Hippo pathway-dependent cytosolic retention of YAP/TAZ (Piccolo et al., 2014). Collectively, these results strongly support the notion that RhoA-mediated cortical actomyosin restrains cell proliferation through the Hippo-YAP/TAZ signal.

Merlin controls Hippo-YAP/TAZ signaling and cell proliferation

To elucidate the molecular mechanism of RhoA-cortical actomyosin-mediated YAP/TAZ nuclear translocation, we focused on merlin, a membrane-cytoskeleton scaffolding protein that interacts with the E-cad complex and F-actin downstream of the RhoA-actomyosin signal (Cooper and Giancotti, 2014). When we knocked down merlin mRNA (more than 30%) using two independent siRNA in mHAT9d cells, YAP/TAZ expression in the nucleus and cell proliferation were facilitated (Fig. 7A-D). Merlin knockdown also reduced cytosolic pYAP and pLATS1/2 expression (Fig. 7E,F), indicating the inactivation of Hippo signaling. These results suggested that merlin mediates between the RhoA-regulated cortical actomyosin and Hippo-dependent YAP/TAZ signal.

DISCUSSION

In this study, we have investigated the impact of microenvironmental O_2 on ESCs using the mouse incisor model and have revealed a signaling axis governing cell proliferation. We have shown that SCCs are located away from blood vessels and are therefore maintained in a relatively hypoxic environment, whereas TACs are found near blood vessels and exist in a relatively high O_2 environment with OXPHOS metabolism. In SCCs, hypoxia-induced HIF1α activated RhoA, which in turn stabilized the cortical actomyosin-AJ protein complex. Merlin at the AJ inhibited YAP/TAZ nuclear translocation through phosphorylation of YAP and LATS1/2, thus resulting in the retention of the slow-cycling state (Fig. 8). These results reveal a unique signal conversion from an environmental stimulus (O_2) to a biochemical transcriptional program (YAP/TAZ) that is integrated by a mechanical stressor (actomyosin), thus highlighting the important implication of blood-vessel geometry for the regulation of ESCs.

The density and geometry of blood vessels have implications on the regulation of DESC behavior

We have observed that SCCs were maintained under relative hypoxia *in vivo* compared with TACs. Interestingly, the apical bud was more distant from the blood vessels than TACs, implying that less O_2 was supplied to SCCs than to TACs. This finding is in line with previous studies that found slow-cycling HSCs residing in the sinusoidal hypoxic zone distant from the vascular niche near the capillaries (Kubota et al., 2008). In neural SCs, relief of hypoxia through the ingrowth of blood vessels promoted their differentiation (Lange et al., 2016). Thus, our findings have shown the important biological implication of the blood-vessel density and geometry for the regulation of ESC behavior, suggesting that the apical bud has a repulsive effect on angiogenesis. Indeed, we have previously demonstrated that the apical bud did not express semaphorin 4D, which has a pro-angiogenic effect (Otsu et al., 2016), whereas other studies have shown that dental epithelial cells (DECs) express semaphorin 3A and 3F, which are anti-angiogenic molecules (Shrestha et al., 2014; Sijaona et al., 2012). These studies strongly suggest the existence of an inter-tissue communication between the apical bud and blood vessels through molecular cues to maintain hypoxia. Therefore, further *in vivo* investigation on deletion/manipulation of blood vessels and direct measurement of oxygen tension will help to identify the correlation between distance from blood vessels and hypoxia, and elucidate the regulatory mechanism underlying blood-vessel density and geometry in the incisor.

A metabolic switch dependent on oxygen concentration is activated in DESCs

TACs were shown to consume more oxygen in the mitochondria than SCCs, to guarantee that sufficient energy (ATP) for active proliferation is available. This suggests that a metabolic switch is activated between SCCs and TACs. Recent studies have shown that the energy requirements in certain SCs are altered depending on the cell lineage, which is supported by mitochondrial biogenesis and the functional change to ensure a suitable amount of ATP (Hu et al., 2016; Ito and Suda, 2014). Under hypoxia, the activity of the mitochondrial electron transport chain is decreased, energetic needs to shift from OXPHOX to glycolysis and, consequently, SCs enhance their self-renewal ability and maintenance of pluripotent capacity *in vitro* (Ježek et al., 2010). For most cell types, hypoxia has been found to decrease the levels of respiratory enzymes and oxygen consumption rate but increase the production of glycolytic enzymes and lactate, which eventually forces the cells to rely on glycolysis (Saini et al., 2013). For example, mesenchymal stem cells (MSCs) have been shown to express higher levels of glycolytic enzymes and lower levels of OXPHOS protein compared with their differentiated progeny (osteoblasts) (Chen et al., 2008). As O_2 concentration increased, MSCs adapted a state of high-oxygen consumption using OXPHOS, and their proliferation increased (Pattappa et al., 2011, 2012). Moreover, intestinal ESCs have been recently reported to exhibit a different metabolic program compared with differentiated cells (Rodríguez-Colman et al., 2017) and with our results. Thus, the importance of this metabolic switch and O_2 in ESCs and its regulatory mechanism should be clarified.

O_2 concentration regulates the RhoA signal in SC regulation

Immunofluorescence assays showed that SCCs resided in a hypoxic environment and exhibited higher HIF1α and active RhoA expression compared with TACs *in vivo*. Also, we have experimentally confirmed that hypoxia induced HIF1α and active RhoA expression, and that HIF1α inhibition reduced active RhoA expression in hypoxia. Other recent studies have also showed the link between hypoxia and the RhoA signal in angiogenesis, endocytosis and the motility of cancer cells (Dada et al., 2007; Gilkes et al., 2014; Turcotte et al., 2003). In normal differentiated cells, such as pulmonary arterial smooth muscle cells and

Development (2021) 148, dev194787. doi:10.1242/dev.194787

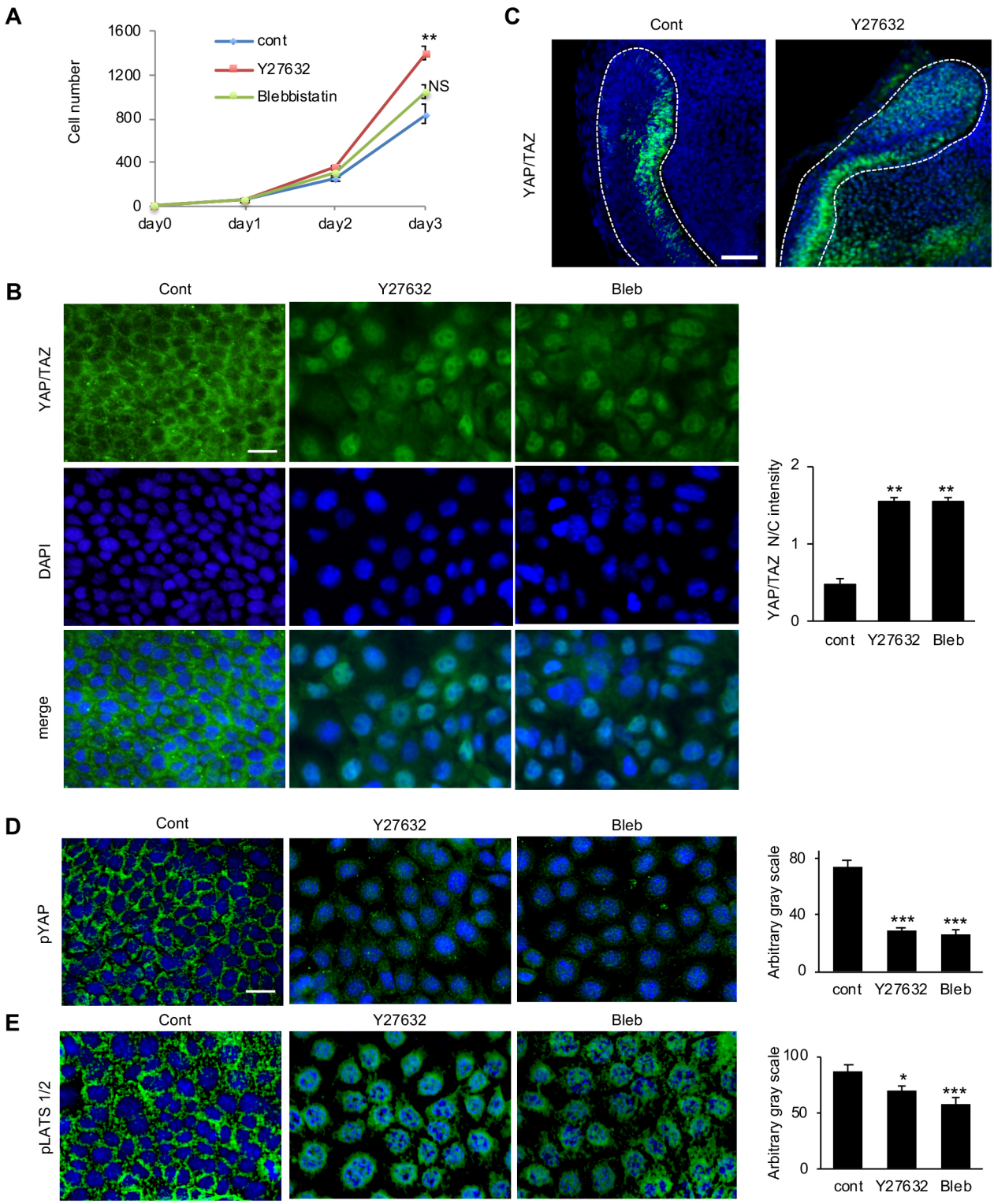

Fig. 6. RhoA/ROCK-mediated cortical actomyosin regulated YAP/TAZ and cell proliferation. (A) mHAT9d cells cultured with vehicle (cont), Y27632 or Blebbistatin (Bleb) were counted using DAPI staining; *n*=4. (B) Immunostaining for YAP/TAZ of high-density mHAT9d cells after treatment with Y27632 and Bleb for 24 h. Quantification (right) of the ratio of nuclear-to-cytosolic (N/C) fluorescence intensity; *n*=5. (C) Immunostaining for YAP/TAZ in control (left) and the apical bud after treatment with Y27632 for 3 days (right). (D,E) Immunostaining for pYAP (S127) (D) and phosphorylated LATS1/2 (pLATS1/2) (E) of high-density mHAT9d cells after treatment with Y27632 and Bleb for 24 h. Quantification of the cytosolic fluorescence intensity; *n*=5. Data are mean±s.e.m. **P*<0.05, ***P*<0.01, ****P*<0.001 (unpaired two-tailed Student's *t*-test). NS, not significant. Scale bars: 20 µm (B,D-E); 50 µm (C).

chondrocytes, RhoA activation by hypoxia has been shown to be involved in actin remodeling and redifferentiation (Bailly et al., 2004; Öztürk et al., 2017). These studies noted that the responsiveness of RhoA to hypoxia was dependent on the cell age and culture condition, implying that impact of O_2 on RhoA signal is context dependent.

Development (2021) 148, dev194787. doi:10.1242/dev.194787

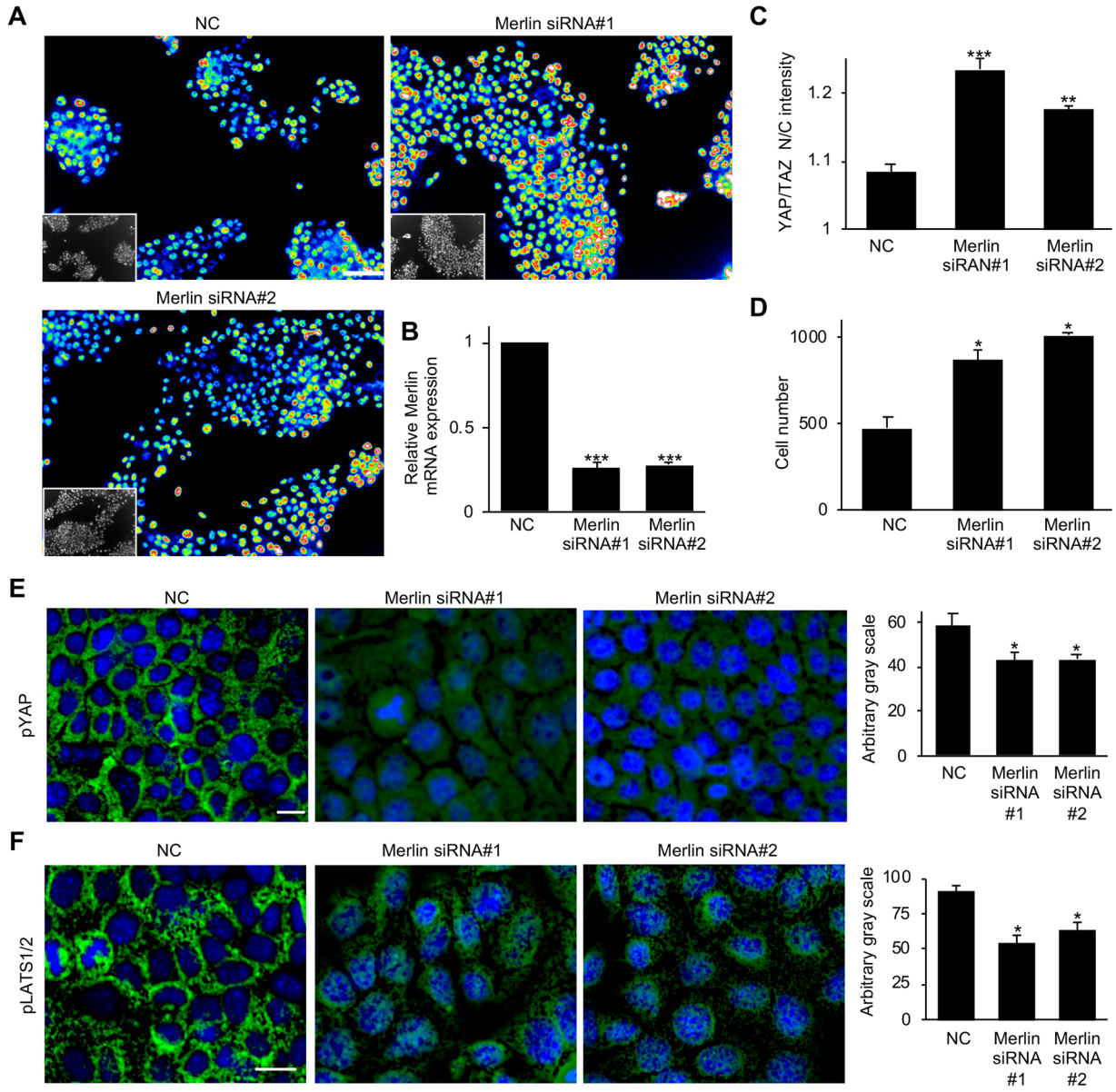

Fig. 7. Effects of knocking down merlin expression in mHAT9d cells. (A) Pseudo-color images show the relative intensity of YAP/TAZ fluorescence in mHAT9d cells transfected with merlin siRNA. Insets are original grayscale images of YAP/TAZ. (B) Expression of merlin mRNA in mHAT9d cells transfected with non-specific control siRNA (NC) or siRNA specific for merlin; n=4. (C) Quantification of the ratio of nuclear-to-cytosolic (N/C) fluorescence intensity; n=4. (D) The cell number was counted using DAPI staining 3 days after merlin siRNA transfection; n=3. Data are represented as mean±s.e.m. (E,F) Immunofluorescence of pYAP (E) or pLATS1/2 (F) of high-density mHAT9d cells transfected with non-specific control siRNA (NC) or two different siRNA specific for merlin. Quantification of the pYAP and pLATS1/2 fluorescence intensities (right); n=3. Data are mean±s.e.m. *P<0.05, **P<0.01, ***P<0.001 (unpaired two-tailed Student's t-test). Scale bars: 100 µm (A); 20 µm (E,F).

Regarding the mechanism by which HIF1α regulates RhoA, certain G-protein-coupled receptors (GPCRs), which modulate RhoA activity, have been shown to be HIF1α target genes (Recchia et al., 2011; Ronkainen et al., 2014), while various GPCR ligands are induced in hypoxia and stimulate RhoGEFs (Stenmark et al., 2006). Conversely, little is known on the involvement of HIF1α in the regulation of RhoGAPs and RhoGDI, which warrants further investigations.

The regulatory mechanism of YAP/TAZ nuclear translocation is dependent on the types of cell and actomyosin

The cortical actomyosin underlying AJ serves as a platform for integrating the chemical and mechanical signals to control many cellular behaviors, including proliferation. Here, we have shown that disruption of the RhoA-mediated cortical actomyosin promoted YAP/TAZ nuclear translocation and cell proliferation via Hippo signaling. We have further confirmed that SCCs, which exhibited high active RhoA, F-actin and pMLC expression, clearly displayed lower YAP/TAZ and YAP1 expression compared with TACs *in vivo*. These findings indicate the crucial role of RhoA-mediated actomyosin on the YAP/TAZ signal to control cell proliferation in DESCs. Consistent with our finding, in MDCK cells the formation of RhoA-mediated cortical actomyosin inhibited YAP/TAZ nuclear translocation and proliferation (Furukawa et al., 2017). On the other hand, other studies using adult transgenic mice showed that another small Rho GTPase, Cdc42, but not the RhoA-ROCK signal, regulated YAP/TAZ localization in DESCs (Hu et al., 2017).

Development (2021) 148, dev194787. doi:10.1242/dev.194787

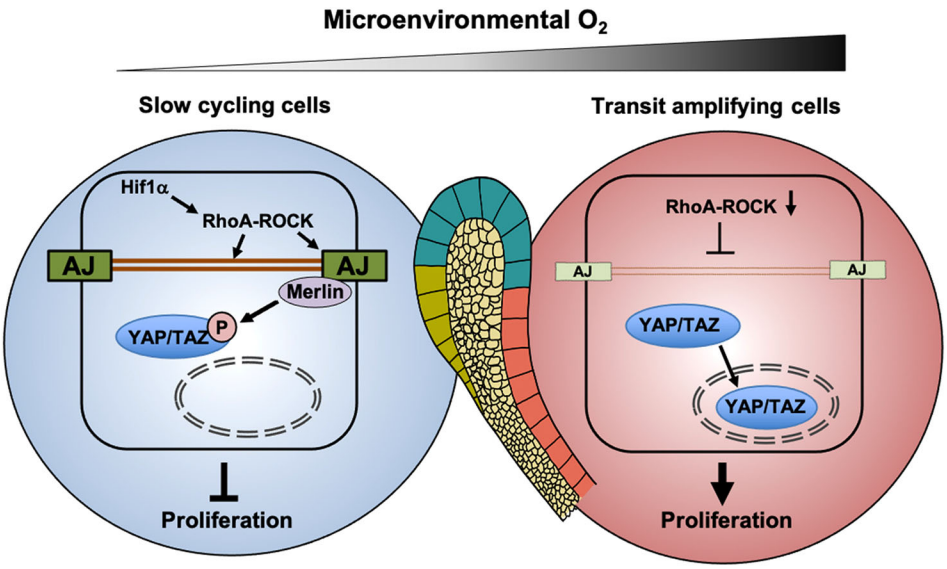

Fig. 8. Model for the regulation of DESC proliferation by O_2. Slow cycling cells (SCCs) located away from the blood vessels are maintained in a relatively hypoxic environment, whereas transit amplifying cells reside near blood vessels and exist in a relatively high O_2 environment. In SCCs, hypoxia facilitates the formation of cortical actomyosin that stabilizes the adherens junction (AJ) complex including merlin through the RhoA signal. Merlin at the AJ suppresses YAP/TAZ nuclear translocation through phosphorylation of YAP to retain a slow-cycling state.

Because our study used neonatal mouse samples, this discrepancy suggests that the type of small GTPase that controls YAP/TAZ may differ depending on age. Further, other cell types have shown the opposite effect of Rho-mediated actomyosin on YAP/TAZ nuclear translocation in stress fibers and primary cilia (Dupont et al., 2011; Kim et al., 2015; Wada et al., 2011), suggesting that the regulatory mechanism of YAP/TAZ by RhoA-mediated actomyosin is cell- and actomyosin-type dependent.

Herein, we have demonstrated that YAP1 was strongly expressed in TACs compared with SCCs, whereas TAZ was expressed in cytosol with no differences between SCCs and TACs *in vivo*. In addition, hypoxia reduced YAP1 mRNA expression, but had no effect on TAZ. These results suggest that YAP and TAZ have non-redundant functions and that YAP1 predominantly contributes to our proposed mechanism under normal conditions. TAZ, expressed in the cytoplasm, is a compensatory effector when YAP activity is disrupted in the mouse incisor (Hu et al., 2017). Hepatic or intestinal deletion of YAP also resulted in TAZ nuclear localization, demonstrating that TAZ became activated in response to YAP loss (Moroishi et al., 2015). Thus, it is inferred that TAZ also play a compensatory role for YAP in our proposed mechanism.

AJ proteins play a role in the proliferation of DESCs

We have showed that Y27632 and blebbistatin caused the disruption of the AJ protein complex, including merlin, and actomyosin breakdown, resulting in the promotion of YAP/TAZ nuclear translocation and cell proliferation. Knocking down merlin inhibited Hippo signaling and promoted YAP/TAZ nuclear translocation and cell proliferation. These results suggest that merlin mediates between RhoA-actomyosin and Hippo-YAP/TAZ signals in DESCs. Consistent with our results, merlin has been reported to regulate YAP/TAZ nuclear translocation through the Hippo pathway via LATS phosphorylation (Yin et al., 2013). However, a recent study has showed that merlin directly controls YAP/TAZ nuclear localization downstream of the cortical actin contraction via nucleocytoplasmic shuttling (Furukawa et al., 2017). This suggests the minor involvement of the direct regulation of YAP/TAZ by merlin in DESCs. In addition to merlin, the strong expression of E-cad in the apical bud has been reported to inhibit the proliferation of DESCs (Li et al., 2012), thus supporting the importance of AJ stability in DESC proliferation.

Contribution of the proposed mechanism to DESCs

We have also observed that the expression patterns of HIF1α, active RhoA, F-actin and merlin were slightly different from pMLC and E-cad in the apical bud. pMLC and E-cad were strongly expressed, whereas the expression of Ki67, YAP/TAZ and YAP1 was weak in SR, which is consistent with our proposed mechanism. Meanwhile, the expression of HIF1α, active RhoA, F-actin and merlin in SR appeared to be relatively weak. This discordance of expression patterns suggests the minor involvement of our proposed mechanism in SCCs within the apical bud, including SR, OEE and BE. However, in comparison between the apical bud and TACs, the expression of HIF1α, active RhoA, pMLC, F-actin, E-cad and merlin in the apical bud were higher than that in TACs, whereas the expression of YAP1, YAP/TAZ and Ki67 were much lower in SCCs than in TACs. These results are in line with the proposed mechanism. Therefore, we concluded that the mechanism proposed in the present study significantly contributed to the regulation of cell proliferation between SCCs and TACs.

In summary, we have demonstrated that microenvironmental O_2 concentrations can fine-tune SC proliferation through RhoA-cortical actomyosin-YAP/TAZ signaling. This finding sheds light on the biological significance of blood-vessel geometry and signal transduction from an O_2 stimulus, mediated by the cytoskeleton, in SC proliferation. Our findings provide a conceptual advance on how SCs interact with their environment during tissue development and renewal, thus aiding in the development of SC-based therapeutic strategies for the regeneration of dental and other ectodermal tissues.

MATERIALS AND METHODS

Animals and tissue preparation

All animal experiments complied with the guidelines of the Ministry of Education, Culture, Sports, Science and Technology, the Ministry of the Environment, and the Science Council of Japan and were carried out in accordance with the Act on Welfare and Management of Animals. The protocol for the animal experiments was approved by the Institutional Animal Care and Use Committee (27-042, 28-028, SA00091) and the Institutional Recombinant DNA Experiments Safety Committee of Iwate Medical University and Niigata University (#308, 406, 423, SD00328).

Animals were maintained in plastic cages inside a room at an ambient temperature of 23±1°C with *ad libitum* access to water and standard laboratory pellet diet. Plug date was defined as E0.5. ddY male mice (RRID: MGI:5558113, Japan SLC, Shizuoka, Japan) were used as the wild type.

Development (2021) 148, dev194787. doi:10.1242/dev.194787

Flk1-GFP BAC Tg mouse (RRID:IMSR_CARD:2408) that were administered with GFP combined with an Flk1 promoter (Ema et al., 2003, 2006; Ishitobi et al., 2010) were used to observe blood vessel distribution. TetOP-H2BGFP mice [B6;129S4-Gt(ROSA)26Sor$^{tm1(rtTA*M2)Jae}$ Col1a1$^{tm7(tetO-HIST1H2BJ/GFP)Jae}$/J *Mus musculus*, RRID:IMSR_JAX:016836] were purchased from the Jackson Laboratory (Foudi et al., 2009). For GFP transgene expression, 2 mg/ml DOX (Merck, D9891, CAS: 24390-14-5) supplemented with 50 mg/ml sucrose was administered to a mother through drinking water to label cell pups at E16.5. Then 3-day-old labeled birthed animals were used to monitor the cell proliferation rate. For histological analysis, mouse jaws were dissected, fixed in 4% paraformaldehyde (PFA; Nacalai Tesque, 26126-25, CAS: 30525-89-4) and decalcified with Osteosoft (Merck, 01728). For Hematoxylin and Eosin (H&E) staining and immunostaining, the samples were dehydrated in a graded ethanol series, embedded in paraffin wax and sectioned (6-7 µm thick) using a microtome (RX-860, Yamato).

Cell culture

mHAT9d cells were established from the apical bud of a mouse incisor (Harada and Ohshima, 2004; Harada and Otsu, 2019; Kawano et al., 2002). The culture medium consisted of Dulbecco's modified Eagle's medium (DMEM)/F12 (11330-032; Life Technologies) supplemented with B-27 (Thermo Fisher Scientific; 17504044), 25 ng/ml basic fibroblast growth factor (FGF) (233-FB; R&D Systems), 20 ng/ml epidermal growth factor (EGF) (2028-EG; R&D Systems) and 1% penicillin-streptomycin (15140; Thermo Fisher Scientific). For comparing low- and high-density cultures, 4×10^4 (low) or 3×10^5 (high) cells for 24-well plates, and 3×10^3 (low) or 5×10^4 (high) cells for 96-well plates were seeded in Corning® Primaria™ culture plates. The cells were treated with (-)-blebbistatin (13013, CAS: 856925-71-8; Cayman Chemical) or Y-27632 (253-00513, CAS: 331752-47-7; Wako). Dimethyl sulfoxide (DMSO; CAS: 67-68-5; Sigma-Aldrich, D2650) and H_2O were used as vehicles for blebbistatin and Y-27632, respectively. To induce hypoxia, the cells were cultured in hypoxic chambers (MCO-5 M, PHCbi) with 5% O_2, 5% CO_2 and 90% N_2. Nitrogen gas was supplied to the chambers to induce a controlled, reduced percentage of oxygen. For normoxia, the cells were cultured in incubators containing 5% CO_2 and 21% O_2.

Mouse incisor organ culture

Mouse incisor organ culture was performed as previously described (Otsu et al., 2016). Briefly, the incisors at P2 were dissected from the lower jaws of ddY mice and grown in a Trowell system. After cultivation with an inhibitor or under hypoxia, the images were taken using a stereomicroscope (Stemi 2000-C, Zeiss) and the explants were then fixed in 4% PFA in PBS, decalcified in Osteosoft, and embedded in paraffin for histological analysis. Image analyses were carried out using ImageJ (https://imagej.nih.gov/ij/).

Immunohistochemistry and immunofluorescence

Immunohistochemical and immunofluorescent staining were performed as described previously (Otsu et al., 2016, 2011). After blocking, the sections were reacted with the following antibodies (1:100): active RhoA (26904, RRID:AB_1961799; NewEast Biosciences), Ki67 (14-5698-82, RRID:AB_10854564; Thermo Fisher Scientific), E-cadherin (610182, RRID:AB_397581; BD Biosciences), F-actin (bs-1571R, RRID:AB_10859354, Bioss), HIF1α (ab16066, RRID:AB_302234; Abcam), p-LATS1/2 (SAB4504615; Merck), Merlin (HPA003097, RRID:AB_1079473; Merck), α-catenin (71-1200, RRID:AB_2533974; Thermo Fisher Scientific), PDH (MA5-14805, RRID:AB_10986167; Thermo Fisher Scientific), citrate synthase (ab96600, RRID:AB_10678258; Abcam), YAP/TAZ (8418, RRID:AB_10950494; Cell Signaling Technology), YAP1 (ab205270, RRID:AB_2813833, Abcam), TAZ (sc-518026; Santa Cruz Biotechnology), pMLC (3671, RRID:AB_330248; Cell Signaling Technology), β-catenin (sc-7963, RRID:AB_626807; Santa Cruz Biotechnology) and pYAP (D9W2I, RRID:AB_2650553; Cell Signaling Technology). DAPI (300 nM; D1306, RRID:AB_2629482), Alexa Fluor 488 (1:500) and Alexa Fluor 546 (1:500) secondary antibodies were procured from Thermo Fisher Scientific. To detect F-actin, the cells were stained using Alexa Fluor 546-conjugated Phalloidin (6.6 µM; A22283, RRID:AB_2632953; Thermo Fisher Scientific). TUNEL staining was conducted using *in situ* apoptosis detection kits according to the manufacturer's protocol (MK500; Takara Bio). Images were obtained under a fluorescence microscope (BX51, IX71, Olympus), laser-scanning confocal microscope (C1si, Nikon) or imaging cytometer (Cytell Cell Imaging System, GE Healthcare UK). Image analyses were carried out using ImageJ or the software provided with the microscope. For the analysis of cell proliferation, cells were imaged using at least 10 fields in every well under ×10 magnification using the Cytell Cell Imaging System, and the imaged nuclei (DAPI fluorescence) were enumerated as the cell number using an image analysis software (IN Cell Analyzer 1000 Workstation, GE Healthcare UK). Appropriate positive and negative controls were run during each experiment.

Scanning electron microscopy

For comparing the mitochondria in SCCs and TACs, we applied array tomography (Micheva and Smith, 2007) with slight modifications. Briefly, the mandibles of TetOP-H2BGFP mice were fixed for 2 h at 4°C in 4% PFA dissolved in 0.1 M phosphate buffer (PB). After three washes with PB, the sample was dehydrated in an ascending series of ethanol (70, 80, 90, 95, 99, 100%), followed by substitution with 1:1 ethanol/LR white resin (AGR1280, CAS #:94188-59-7; Agar Scientific) overnight at room temperature (20∼25°C). Final infiltration with LR white resin was carried out. Polymerization was performed by incubation at 60°C for 3 days. The resin-embedded samples were cut into ultrathin sections (0.5 µm thickness) using a Histo Diamond Knife (Diatome) and then bonded to glass slides. GFP fluorescence in the sections was imaged using a laser-scanning confocal microscope (C1si). The same sections were then stained with 1% uranyl acetate in H_2O for 30 min and with lead stain solution (18-08-75-2; Merck) and imaged on an SU-8010 electron microscope (Hitachi High-Technologies). SCCs and TACs were classified based on the GFP intensity in the fluorescent image, and their mitochondria were analyzed using SEM images. Image analyses were carried out using ImageJ.

Immunoblotting

Immunoblotting was performed as previously described (Ida-Yonemochi et al., 2016). After incubation under hypoxic condition for 24 h, mHAT9d cells were lysed using RIPA buffer (08714-04; Nacalai Tesque). The lysates were separated using SDS-PAGE and transferred to PVDF membranes. The membranes were incubated with anti-HIF1α antibody (1:1000) or α-tubulin (1:1000; 66031-1-lg, RRID:AB_11042766; Proteintech). For immunodetection, the Envision+/HRP system (K4061; Dako) was used, and the antigens were detected using Western BLoT Quant HRP Substrate (T7102A; Takara Bio).

siRNA

Sets of two 25-mer duplex siRNAs targeting genes were obtained from Thermo Fisher Scientific. All siRNA duplexes (10 nmol/l) were transfected into cells using Lipofectamine RNAiMAX (13778075; Thermo Fisher Scientific) according to the manufacturer's protocol. Stealth siRNA negative control duplexes (12935300; Thermo Fisher Scientific) were used to control for the sequence-independent effects following siRNA delivery. Transfection efficiency, which was monitored using a fluorescent oligonucleotide (14750100, BLOCK-iT fluorescent oligonucleotide; Thermo Fisher Scientific), was estimated to be between 80% and 90%. Inhibitory effects were observed in all siRNA duplexes, and two of the three siRNAs with strong inhibitory effect were used in three independent experiments.

RT-qPCR

Total RNA was extracted using an RNeasy Mini Kit (74104; Qiagen). Reverse transcription of the total RNA was performed using a PrimeScript RT reagent kit (RR037A; Takara Bio). The quantitative analysis of gene expression was performed through RT-qPCR using SYBR1 Premix Ex Taq (RR820S; Takara Bio) and the oligonucleotide primers specific for the target sequences on a Thermal Cycler Dice (Takara Bio) according to the

manufacturer's protocol. Amplification conditions were as follows: 30 s at 95°C; 40 cycles of 95°C for 5 s and 60°C for 30 s; dissociation for 15 s at 95°C; and 30 s at 60°C. Target gene expression levels were normalized against the corresponding levels of Gapdh mRNA. The relative gene expression levels were calculated against the values of the negative control cultures using the comparative Ct ($2^{-\Delta\Delta Ct}$) method. Experiments were carried out in triplicate. Sequences of primers are as follows: Gapdh (Fw 5′-TGTGTCCGTCGTGGATCTGA-3′, Rv 5′-TTGCTGTTGAAGTCGCA-GGAG-3′), E-cad (Fw 5′-CGTCCTGCCAATCCTGATGA-3′, Rv 5′-AC-CACTGCCCTCGTAATCGAAC-3′), HIF1α (Fw 5′-GCGTGCATGTCT-AATCTGTTCC-3′, Rv 5′-GATTCTGACATGCCACATAGCTC-3′), merlin (Fw 5′-GAAGCTCTTAGAAATCGCCACCA-3′, Rv 5′-CAGCA-ATAATGTCGAAGCTCGGTA-3′), YAP1 (Fw 5′-CATGGTGCGCC-TT-GTTATACCTC-3′, Rv 5′-TCAGGCCGTGATTCAAATTTAGTG-3′), TAZ (Fw 5′-TCACCGTCTCCAACCACCAG-3′, Rv 5′-AGCTCCTTGG-TGAAGCAGATGTC-3′).

Statistical analysis

All data are mean±s.e.m. Differences were considered statistically significant if $P<0.05$ using unpaired two-tailed Student's *t*-test: *$P<0.05$, **$P<0.01$, ***$P<0.001$. To quantify the immunofluorescence intensity, at least 30 cells in every sample were analyzed in one experiment unless otherwise indicated.

Acknowledgements

We thank Naoyuki Nishiya (Department of Clinical Pharmacy, Iwate Medical University) for useful discussions regarding our study and for helpful insights. We also thank Tomohito Hanasaka and Eri Ishiyama (Technical Support Center for Life Science Research, Iwate Medical University), and Takafumi Fukasawa, Wataru Yasuno (Center for In Vivo Science, Iwate Medical University) and Aya Kikuchi for technical assistance, and Yukiko Onuma and Michiko Sugawara for secretarial support.

Competing interests

The authors declare no competing or financial interests.

Author contributions

Conceptualization: K.O., H.H.; Methodology: K.O., H.H.; Validation: K.O., H.H.; Formal analysis: K.O.; Investigation: K.O., H.I.-Y., S.I., H.O., H.H.; Resources: M.E., J.H., H.O.; Writing - original draft: K.O.; Writing - review & editing: H.I.-Y., H.O., H.H.; Visualization: K.O.; Supervision: H.H.; Project administration: H.H.; Funding acquisition: K.O., H.H.

Funding

This work was financially supported by: the Japan Society for the Promotion of Science KAKENHI [JP18K09526 and JP26462794 to K.O., JP18H02984 and JP16K15813 to H.H. and JP17H04366 to H.O.]; the Japan Society for the Promotion of Science and National Research Foundation of Korea under the Japan-Korea Basic Scientific Cooperation Program (2018-2020) to K.O.; and the KEIRYOKAI Research grant (Collaborative project 2017-2019) to K.O.

Supplementary information

Supplementary information available online at
https://dev.biologists.org/lookup/doi/10.1242/dev.194787.supplemental

Peer review history

The peer review history is available online at
https://dev.biologists.org/lookup/doi/10.1242/dev.194787.reviewer-comments.pdf

References

Bailly, K., Ridley, A. J., Hall, S. M. and Haworth, S. G. (2004). RhoA activation by hypoxia in pulmonary arterial smooth muscle cells is age and site specific. *Circ. Res.* **94**, 1383-1391. doi:10.1161/01.RES.0000128405.83582.2e

Camargo, F. D., Gokhale, S., Johnnidis, J. B., Fu, D., Bell, G. W., Jaenisch, R. and Brummelkamp, T. R. (2007). YAP1 increases organ size and expands undifferentiated progenitor cells. *Curr. Biol.* **17**, 2054-2060. doi:10.1016/j.cub.2007.10.039

Cao, X., Pfaff, S. L. and Gage, F. H. (2008). YAP regulates neural progenitor cell number via the TEA domain transcription factor. *Genes Dev.* **22**, 3320-3334. doi:10.1101/gad.1726608

Chen, C.-T., Shih, Y.-R. V., Kuo, T. K., Lee, O. K. and Wei, Y.-H. (2008). Coordinated changes of mitochondrial biogenesis and antioxidant enzymes during osteogenic differentiation of human mesenchymal stem cells. *Stem Cells* **26**, 960-968. doi:10.1634/stemcells.2007-0509

Chen, T., Heller, E., Beronja, S., Oshimori, N., Stokes, N. and Fuchs, E. (2012). An RNA interference screen uncovers a new molecule in stem cell self-renewal and long-term regeneration. *Nature* **485**, 104-108. doi:10.1038/nature10940

Cheng, T.-L., Liao, C.-C., Tsai, W.-H., Lin, C.-C., Yeh, C.-W., Teng, C.-F. and Chang, W.-T. (2009). Identification and characterization of the mitochondrial targeting sequence and mechanism in human citrate synthase. *J. Cell. Biochem.* **107**, 1002-1015. doi:10.1002/jcb.22200

Choi, W., Kwon, S.-J., Jin, H. J., Jeong, S. Y., Choi, S. J., Oh, W., Yang, Y. S., Jeon, H. B. and Jeon, E. S. (2017). Optimization of culture conditions for rapid clinical-scale expansion of human umbilical cord blood-derived mesenchymal stem cells. *Clin. Transl. Med.* **6**, e38. doi:10.1186/s40169-017-0168-z

Coleman, M. L., Marshall, C. J. and Olson, M. F. (2004). RAS and RHO GTPases in G1-phase cell-cycle regulation. *Nat. Rev. Mol. Cell Biol.* **5**, 355-366. doi:10.1038/nrm1365

Cooper, J. and Giancotti, F. G. (2014). Molecular insights into NF2/Merlin tumor suppressor function. *FEBS Lett.* **588**, 2743-2752. doi:10.1016/j.febslet.2014.04.001

Csete, M. (2005). Oxygen in the cultivation of stem cells. *Ann. N. Y. Acad. Sci.* **1049**, 1-8. doi:10.1196/annals.1334.001

Dada, L. A., Novoa, E., Lecuona, E., Sun, H. and Sznajder, J. I. (2007). Role of the small GTPase RhoA in the hypoxia-induced decrease of plasma membrane Na, K-ATPase in A549 cells. *J. Cell Sci.* **120**, 2214-2222. doi:10.1242/jcs.003038

Dong, J., Feldmann, G., Huang, J., Wu, S., Zhang, N., Comerford, S. A., Gayyed, M. F., Anders, R. A., Maitra, A. and Pan, D. (2007). Elucidation of a universal size-control mechanism in *Drosophila* and mammals. *Cell* **130**, 1120-1133. doi:10.1016/j.cell.2007.07.019

Dupont, S., Morsut, L., Aragona, M., Enzo, E., Giulitti, S., Cordenonsi, M., Zanconato, F., Le Digabel, J., Forcato, M., Bicciato, S. et al. (2011). Role of YAP/TAZ in mechanotransduction. *Nature* **474**, 179. doi:10.1038/nature10137

Ema, M., Faloon, P., Zhang, W. J., Hirashima, M., Reid, T., Stanford, W. L., Orkin, S., Choi, K. and Rossant, J. (2003). Combinatorial effects of Flk1 and Tal1 on vascular and hematopoietic development in the mouse. *Genes Dev.* **17**, 380-393. doi:10.1101/gad.1049803

Ema, M., Takahashi, S. and Rossant, J. (2006). Deletion of the selection cassette, but not cis-acting elements, in targeted Flk1-lacZ allele reveals Flk1 expression in multipotent mesodermal progenitors. *Blood* **107**, 111-117. doi:10.1182/blood-2005-05-1970

Foudi, A., Hochedlinger, K., Van Buren, D., Schindler, J. W., Jaenisch, R., Carey, V. and Hock, H. (2009). Analysis of histone 2B-GFP retention reveals slowly cycling hematopoietic stem cells. *Nat. Biotechnol.* **27**, 84-90. doi:10.1038/nbt.1517

Furukawa, K. T., Yamashita, K., Sakurai, N. and Ohno, S. (2017). The epithelial circumferential actin belt regulates YAP/TAZ through nucleocytoplasmic shuttling of merlin. *Cell Rep.* **20**, 1435-1447. doi:10.1016/j.celrep.2017.07.032

Gilkes, D. M., Xiang, L., Lee, S. J., Chaturvedi, P., Hubbi, M. E., Wirtz, D. and Semenza, G. L. (2014). Hypoxia-inducible factors mediate coordinated RhoA-ROCK1 expression and signaling in breast cancer cells. *Proc. Natl. Acad. Sci. USA* **111**, E384-E393. doi:10.1073/pnas.1321510111

Gustafsson, M. V., Zheng, X., Pereira, T., Gradin, K., Jin, S., Lundkvist, J., Ruas, J. L., Poellinger, L., Lendahl, U. and Bondesson, M. (2005). Hypoxia requires notch signaling to maintain the undifferentiated cell state. *Dev. Cell* **9**, 617-628. doi:10.1016/j.devcel.2005.09.010

Harada, H. and Ohshima, H. (2004). New perspectives on tooth development and the dental stem cell niche. *Arch. Histol. Cytol.* **67**, 1-11. doi:10.1679/aohc.67.1

Harada, H. and Otsu, K. (2019). Microdissection and isolation of mouse dental epithelial cells of continuously growing mouse incisors. In *Odontogenesis: Methods and Protocols* and (ed. P. Papagerakis), pp. 3-11. New York, NY: Springer New York.

Harada, H., Kettunen, P., Jung, H.-S., Mustonen, T., Wang, Y. A. and Thesleff, I. (1999). Localization of putative stem cells in dental epithelium and their association with notch and FGF signaling. *J. Cell Biol.* **147**, 105-120. doi:10.1083/jcb.147.1.105

Harris, R. A., Bowker-Kinley, M. M., Huang, B. and Wu, P. (2002). Regulation of the activity of the pyruvate dehydrogenase complex. *Adv. Enzyme Regul.* **42**, 249. doi:10.1016/S0065-2571(01)00061-9

Hsu, Y.-C., Li, L. and Fuchs, E. (2014). Transit-amplifying cells orchestrate stem cell activity and tissue regeneration. *Cell* **157**, 935-949. doi:10.1016/j.cell.2014.02.057

Hu, C., Fan, L., Cen, P., Chen, E., Jiang, Z. and Li, L. (2016). Energy metabolism plays a critical role in stem cell maintenance and differentiation. *Int. J. Mol. Sci.* **17**, 253. doi:10.3390/ijms17020253

Hu, J. K.-H., Du, W., Shelton, S. J., Oldham, M. C., DiPersio, C. M. and Klein, O. D. (2017). An FAK-YAP-mTOR signaling axis regulates stem cell-based tissue renewal in mice. *Cell Stem Cell* **21**, 91-106.e6. doi:10.1016/j.stem.2017.03.023

Ida-Yonemochi, H., Otsu, K., Ohshima, H. and Harada, H. (2016). The glycogen metabolism via Akt signaling is important for the secretion of enamel matrix in tooth development. *Mech. Dev.* **139**, 18-30. doi:10.1016/j.mod.2016.01.002
Ishitobi, H., Matsumoto, K., Azami, T., Itoh, F., Itoh, S., Takahashi, S. and Ema, M. (2010). Flk1-GFP BAC Tg mice: an animal model for the study of blood vessel development. *Exp. Anim.* **59**, 615-622. doi:10.1538/expanim.59.615
Ito, K. and Suda, T. (2014). Metabolic requirements for the maintenance of self-renewing stem cells. *Nat. Rev. Mol. Cell Biol.* **15**, 243-256. doi:10.1038/nrm3772
Jaffe, A. B. and Hall, A. (2005). Rho GTPases: biochemistry and biology. *Annu. Rev. Cell Dev. Biol.* **21**, 247-269. doi:10.1146/annurev.cellbio.21.020604.150721
Ježek, P., Plecitá-Hlavatá, L., Smolková, K. and Rossignol, R. (2010). Distinctions and similarities of cell bioenergetics and the role of mitochondria in hypoxia, cancer, and embryonic development. *Int. J. Biochem. Cell Biol.* **42**, 604-622. doi:10.1016/j.biocel.2009.11.008
Juuri, E., Saito, K., Ahtiainen, L., Seidel, K., Tummers, M., Hochedlinger, K., Klein, O. D., Thesleff, I. and Michon, F. (2012). Sox2+ stem cells contribute to all epithelial lineages of the tooth via Sfrp5+ progenitors. *Dev. Cell* **23**, 317-328. doi:10.1016/j.devcel.2012.05.012
Kawano, S., Morotomi, T., Toyono, T., Nakamura, N., Uchida, T., Ohishi, M., Toyoshima, K. and Harada, H. (2002). Establishment of dental epithelial cell line (HAT-7) and the cell differentiation dependent on notch signaling pathway. *Connect. Tissue Res.* **43**, 409-412. doi:10.1080/03008200290000637
Kim, J., Jo, H., Hong, H., Kim, M. H., Kim, J. M., Lee, J.-K., Do Heo, W. and Kim, J. (2015). Actin remodelling factors control ciliogenesis by regulating YAP/TAZ activity and vesicle trafficking. *Nat. Commun.* **6**, 6781. doi:10.1038/ncomms7781
Kuang-Hsien Hu, J., Mushegyan, V. and Klein, O. D. (2014). On the cutting edge of organ renewal: identification, regulation, and evolution of incisor stem cells. *Genesis* **52**, 79-92. doi:10.1002/dvg.22732
Kubota, Y., Takubo, K. and Suda, T. (2008). Bone marrow long label-retaining cells reside in the sinusoidal hypoxic niche. *Biochem. Biophys. Res. Commun.* **366**, 335-339. doi:10.1016/j.bbrc.2007.11.086
Lange, C., Turrero Garcia, M., Decimo, I., Bifari, F., Eelen, G., Quaegebeur, A., Boon, R., Zhao, H., Boeckx, B., Chang, J. et al. (2016). Relief of hypoxia by angiogenesis promotes neural stem cell differentiation by targeting glycolysis. *EMBO J.* **35**, 924-941. doi:10.15252/embj.201592372
Lecuit, T. and Yap, A. S. (2015). E-cadherin junctions as active mechanical integrators in tissue dynamics. *Nat. Cell Biol.* **17**, 533-539. doi:10.1038/ncb3136
Lei, Q.-Y., Zhang, H., Zhao, B., Zha, Z.-Y., Bai, F., Pei, X.-H., Zhao, S., Xiong, Y. and Guan, K.-L. (2008). TAZ promotes cell proliferation and epithelial-mesenchymal transition and is inhibited by the hippo pathway. *Mol. Cell. Biol.* **28**, 2426-2436. doi:10.1128/MCB.01874-07
Li, C.-Y., Cha, W., Luder, H.-U., Charles, R.-P., McMahon, M., Mitsiadis, T. A. and Klein, O. D. (2012). E-cadherin regulates the behavior and fate of epithelial stem cells and their progeny in the mouse incisor. *Dev. Biol.* **366**, 357-366. doi:10.1016/j.ydbio.2012.03.012
Lin, Q., Kim, Y., Alarcon, R. M. and Yun, Z. (2008). Oxygen and cell fate decisions. *Gene Regul. Syst. Bio.* **2**, 43-51. doi:10.4137/GRSB.S434
Micheva, K. D. and Smith, S. J. (2007). Array tomography: a new tool for imaging the molecular architecture and ultrastructure of neural circuits. *Neuron* **55**, 25-36. doi:10.1016/j.neuron.2007.06.014
Mohyeldin, A., Garzón-Muvdi, T. and Quiñones-Hinojosa, A. (2010). Oxygen in stem cell biology: a critical component of the stem cell niche. *Cell Stem Cell* **7**, 150-161. doi:10.1016/j.stem.2010.07.007
Moroishi, T., Park, H. W., Qin, B., Chen, Q., Meng, Z., Plouffe, S. W., Taniguchi, K., Yu, F.-X., Karin, M., Pan, D. et al. (2015). A YAP/TAZ-induced feedback mechanism regulates Hippo pathway homeostasis. *Genes Dev.* **29**, 1271-1284. doi:10.1101/gad.262816.115
Morrison, S. J. and Spradling, A. C. (2008). Stem cells and niches: mechanisms that promote stem cell maintenance throughout life. *Cell* **132**, 598-611. doi:10.1016/j.cell.2008.01.038
Otsu, K., Kishigami, R., Fujiwara, N., Ishizeki, K. and Harada, H. (2011). Functional role of rho–kinase in ameloblast differentiation. *J. Cell. Physiol.* **226**, 2527-2534. doi:10.1002/jcp.22597
Otsu, K., Ida-Yonemochi, H., Fujiwara, N. and Harada, H. (2016). The Semaphorin 4D-RhoA-Akt signal cascade regulates enamel matrix secretion in coordination with cell polarization during ameloblast differentiation. *J. Bone Miner. Res.* **31**, 1943-1954. doi:10.1002/jbmr.2876
Öztürk, E., Hobiger, S., Despot-Slade, E., Pichler, M. and Zenobi-Wong, M. (2017). Hypoxia regulates RhoA and Wnt/β-catenin signaling in a context-dependent way to control re-differentiation of chondrocytes. *Sci. Rep.* **7**, 9032. doi:10.1038/s41598-017-09505-6
Pattappa, G., Heywood, H. K., De Bruijn, J. D. and Lee, D. A. (2011). The metabolism of human mesenchymal stem cells during proliferation and differentiation. *J. Cell. Physiol.* **226**, 2562-2570. doi:10.1002/jcp.22605
Pattappa, G., Thorpe, S. D., Jegard, N. C., Heywood, H. K., de Bruijn, J. D. and Lee, D. A. (2012). Continuous and uninterrupted oxygen tension influences the colony formation and oxidative metabolism of human mesenchymal stem cells. *Tissue Eng. Part C: Methods* **19**, 68-79. doi:10.1089/ten.tec.2011.0734
Piccolo, S., Dupont, S. and Cordenonsi, M. (2014). The biology of YAP/TAZ: hippo signaling and beyond. *Physiol. Rev.* **94**, 1287-1312. doi:10.1152/physrev.00005.2014
Pietras, E. M., Warr, M. R. and Passegué, E. (2011). Cell cycle regulation in hematopoietic stem cells. *J. Cell Biol.* **195**, 709-720. doi:10.1083/jcb.201102131
Recchia, A. G., De Francesco, E. M., Vivacqua, A., Sisci, D., Panno, M. L., Andò, S. and Maggiolini, M. (2011). The G protein-coupled receptor 30 is up-regulated by hypoxia-inducible factor-1α (HIF-1α) in breast cancer cells and cardiomyocytes. *J. Biol. Chem.* **286**, 10773-10782. doi:10.1074/jbc.M110.172247
Ridley, A. J. (1996). Rho: theme and variations. *Curr. Biol.* **6**, 1256-1264. doi:10.1016/S0960-9822(02)70711-2
Riento, K. and Ridley, A. J. (2003). Rocks: multifunctional kinases in cell behaviour. *Nat. Rev. Mol. Cell Biol.* **4**, 446-456. doi:10.1038/nrm1128
Rodríguez-Colman, M. J., Schewe, M., Meerlo, M., Stigter, E., Gerrits, J., Pras-Raves, M., Sacchetti, A., Hornsveld, M., Oost, K. C. and Snippert, H. J. et al. (2017). Interplay between metabolic identities in the intestinal crypt supports stem cell function. *Nature* **543**, 424. doi:10.1038/nature21673
Ronkainen, V.-P., Tuomainen, T., Huusko, J., Laidinen, S., Malinen, M., Palvimo, J. J., Ylä-Herttuala, S., Vuolteenaho, O. and Tavi, P. (2014). Hypoxia-inducible factor 1-induced G protein-coupled receptor 35 expression is an early marker of progressive cardiac remodelling. *Cardiovasc. Res.* **101**, 69-77. doi:10.1093/cvr/cvt226
Saini, U., Gumina, R. J., Wolfe, B., Kuppusamy, M. L., Kuppusamy, P. and Boudoulas, K. D. (2013). Preconditioning mesenchymal stem cells with caspase inhibition and hyperoxia prior to hypoxia exposure increases cell proliferation. *J. Cell. Biochem.* **114**, 2612-2623. doi:10.1002/jcb.24609
Schlegelmilch, K., Mohseni, M., Kirak, O., Pruszak, J., Rodriguez, J. R., Zhou, D., Kreger, B. T., Vasioukhin, V., Avruch, J. and Brummelkamp, T. R. et al. (2011). Yap1 acts downstream of α-catenin to control epidermal proliferation. *Cell* **144**, 782-795. doi:10.1016/j.cell.2011.02.031
Seidel, K., Marangoni, P., Tang, C., Houshmand, B., Du, W., Maas, R. L., Murray, S., Oldham, M. C. and Klein, O. D. (2017). Resolving stem and progenitor cells in the adult mouse incisor through gene co-expression analysis. *eLife* **6**, e24712. doi:10.7554/eLife.24712
Sharir, A., Marangoni, P., Zilionis, R., Wan, M., Wald, T., Hu, J. K., Kawaguchi, K., Castillo-Azofeifa, D., Epstein, L., Harrington, K. et al. (2019). A large pool of actively cycling progenitors orchestrates self-renewal and injury repair of an ectodermal appendage. *Nat. Cell Biol.* **21**, 1102-1112. doi:10.1038/s41556-019-0378-2
Shrestha, A., Moe, K., Luukko, K., Taniguchi, M. and Kettunen, P. (2014). Sema3A chemorepellant regulates the timing and patterning of dental nerves during development of incisor tooth germ. *Cell Tissue Res.* **357**, 15-29. doi:10.1007/s00441-014-1839-3
Sijaona, A., Luukko, K., Kvinnsland, I. H. and Kettunen, P. (2012). Expression patterns of Sema3F, PlexinA4,-A3, Neuropilin1 and –2 in the postnatal mouse molar suggest roles in tooth innervation and organogenesis. *Acta Odontol. Scand.* **70**, 140-148. doi:10.3109/00016357.2011.600708
Simon, M. C. and Keith, B. (2008). The role of oxygen availability in embryonic development and stem cell function. *Nat. Rev. Mol. Cell Biol.* **9**, 285-296. doi:10.1038/nrm2354
Stenmark, K. R., Fagan, K. A. and Frid, M. G. (2006). Hypoxia-induced pulmonary vascular remodeling: cellular and molecular mechanisms. *Circ. Res.* **99**, 675-691. doi:10.1161/01.RES.0000243584.45145.3f
Takubo, K., Goda, N., Yamada, W., Iriuchishima, H., Ikeda, E., Kubota, Y., Shima, H., Johnson, R. S., Hirao, A., Suematsu, M. et al. (2010). Regulation of the HIF-1α level is essential for hematopoietic stem cells. *Cell Stem Cell* **7**, 391-402. doi:10.1016/j.stem.2010.06.020
Turcotte, S., Desrosiers, R. R. and Béliveau, R. (2003). HIF-1α mRNA and protein upregulation involves Rho GTPase expression during hypoxia in renal cell carcinoma. *J. Cell Sci.* **116**, 2247-2260. doi:10.1242/jcs.00427
Wabik, A. and Jones, P. H. (2015). Switching roles: the functional plasticity of adult tissue stem cells. *EMBO J.* **34**, 1164-1179. doi:10.15252/embj.201490386
Wada, K.-I., Itoga, K., Okano, T., Yonemura, S. and Sasaki, H. (2011). Hippo pathway regulation by cell morphology and stress fibers. *Development* **138**, 3907-3914. doi:10.1242/dev.070987
Watt, K. I., Judson, R., Medlow, P., Reid, K., Kurth, T. B., Burniston, J. G., Ratkevicius, A., De Bari, C. and Wackerhage, H. (2010). Yap is a novel regulator of C2C12 myogenesis. *Biochem. Biophys. Res. Commun.* **393**, 619-624. doi:10.1016/j.bbrc.2010.02.034
Yin, F., Yu, J., Zheng, Y., Chen, Q., Zhang, N. and Pan, D. (2013). Spatial organization of Hippo signaling at the plasma membrane mediated by the tumor suppressor Merlin/NF2. *Cell* **154**, 1342-1355. doi:10.1016/j.cell.2013.08.025
Yu, T. and Klein, O. D. (2020). Molecular and cellular mechanisms of tooth development, homeostasis and repair. *Development* **147**, dev184754. doi:10.1242/dev.184754
Zhao, B., Wei, X., Li, W., Udan, R. S., Yang, Q., Kim, J., Xie, J., Ikenoue, T., Yu, J. and Li, L. et al. (2007). Inactivation of YAP oncoprotein by the Hippo pathway is involved in cell contact inhibition and tissue growth control. *Genes Dev.* **21**, 2747-2761. doi:10.1101/gad.1602907

Supplementary Fig. 1

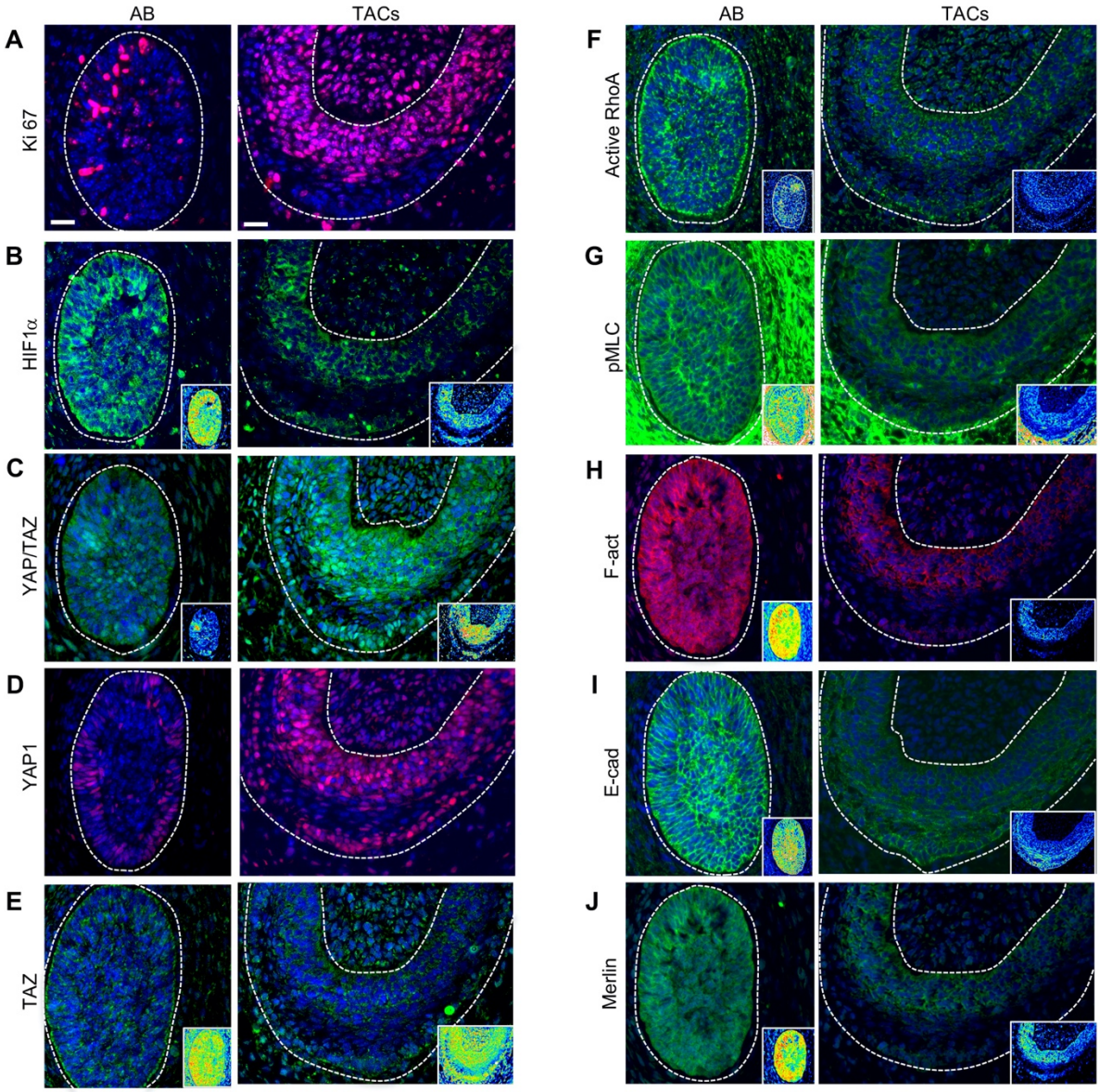

Figure S1. Immunostaining of adjacent frontal sections of mouse incisor *in vivo*

(A-J) Immunostaining of Ki67, HIF1α, YAP/TAZ, YAP1, TAZ, Active RhoA, pMLC, F-actin, E-cadherin, and Merlin in adjacent frontal sections of apical bud (AB) region (left) and TACs region (TACs) (right) of the same P3 mouse lower incisor. The nucleus is stained with DAPI (blue). Insets are pseudo-color images; dashed line delimits the dental epithelium. Scale bars: 20 μm.

Supplementary Fig.2

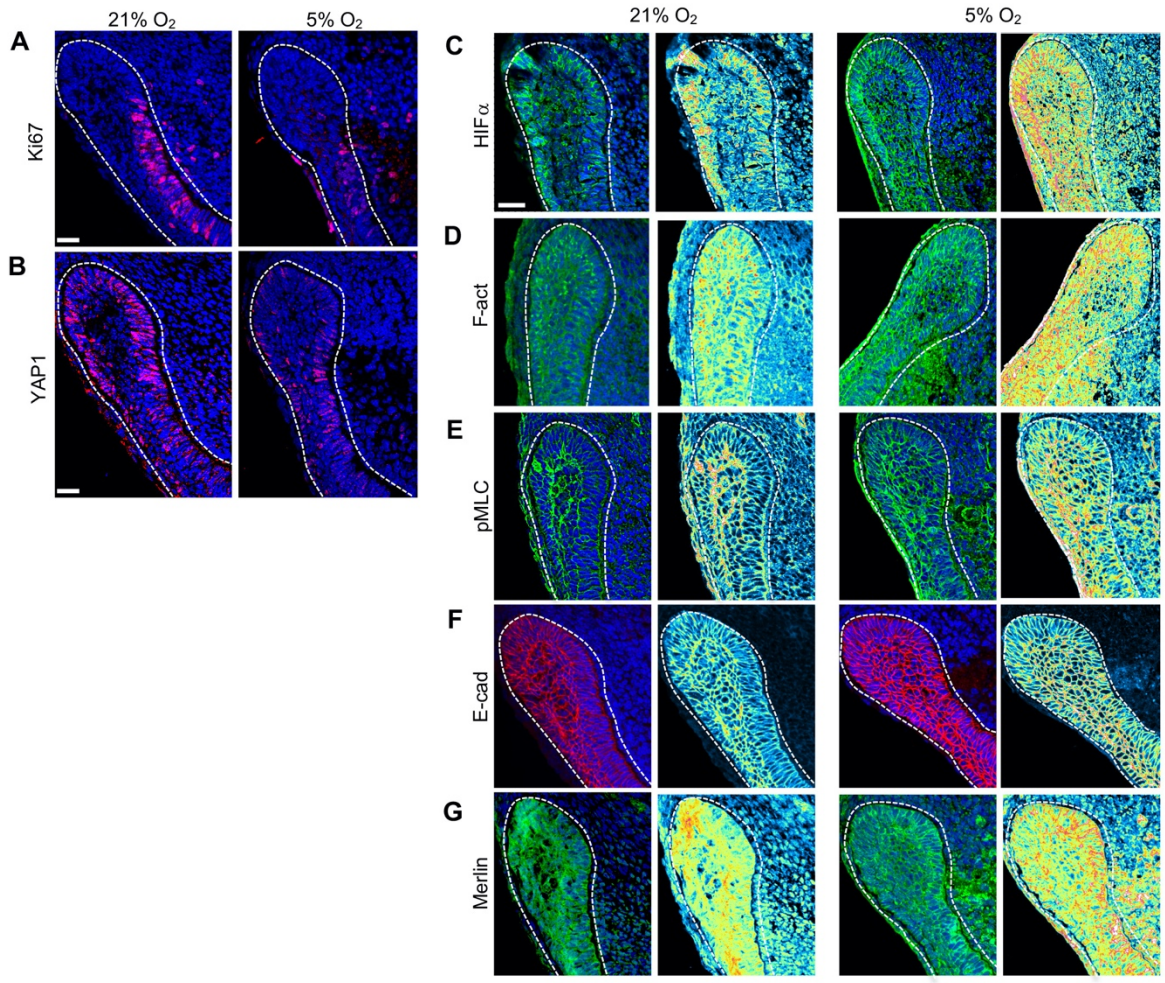

Figure S2. Immunostaining of adjacent sagittal sections of cultured mouse incisors in hypoxia

(A-G) Immunostaining of Ki67, YAP1, HIF1α, F-actin, pMLC, E-cadherin, and Merlin in adjacent sagittal sections of the apical bud cultured in normoxia and hypoxia. The nucleus is stained with DAPI (blue). (C-G) Right images are pseudo-color images of left images; dashed line delimits the dental epithelium. Scale bars: 20 μm.

Supplementary Fig.3

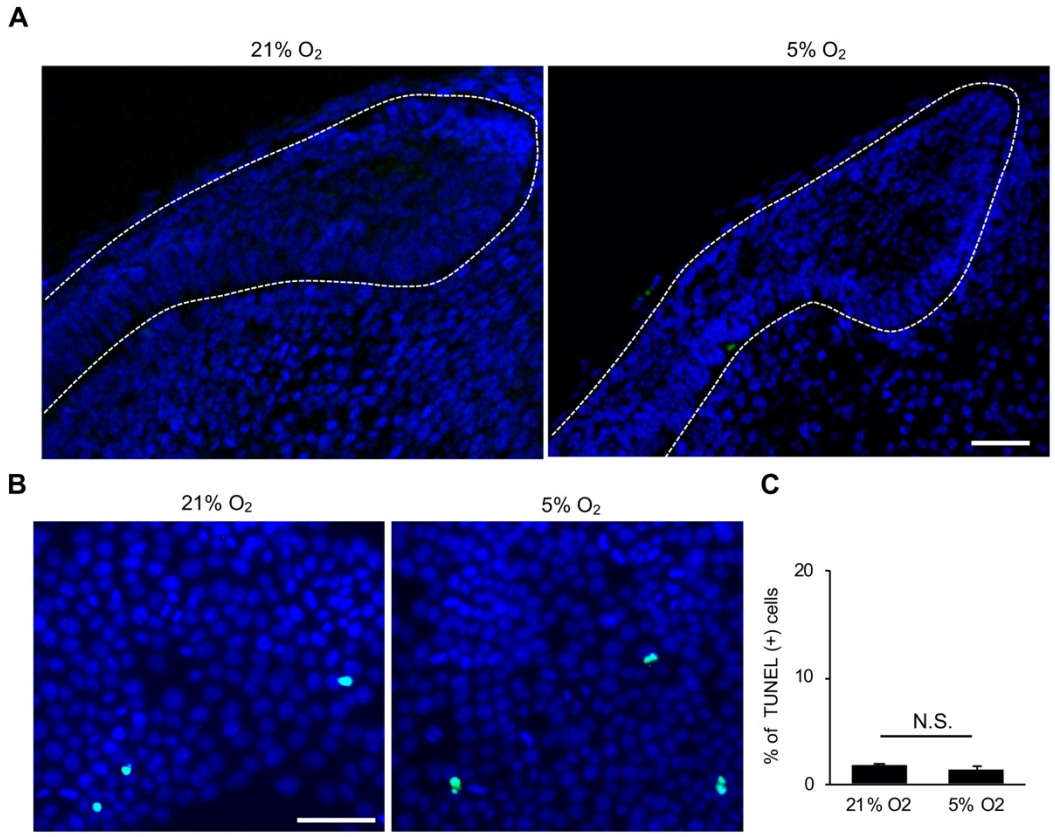

Figure S3. Effect of hypoxia on apoptosis in cultured mouse incisors and mHAT9d cells. (A) Terminal deoxynucleotidyl transferase (TdT)-mediated dUTP-biotin nick-end labeling (TUNEL) staining assay of the apical bud cultured in normoxia (left) and hypoxia (right) for 2 days. (B, C) TUNEL staining assay of mHAT9d cells incubated in normoxia (21% O_2) or hypoxia (5% O_2) for 1 day. Representative images demonstrate TUNEL-positive nuclei (green color). The nucleus is stained with DAPI (blue). Percentages (%) of TUNEL-positive cells relative to DAPI-positive total nuclei are indicated in the histogram; n = 4. N.S., non-significant. Scale bars: (A) 30 μm; (B) 50 μm.

Supplementary Fig.4

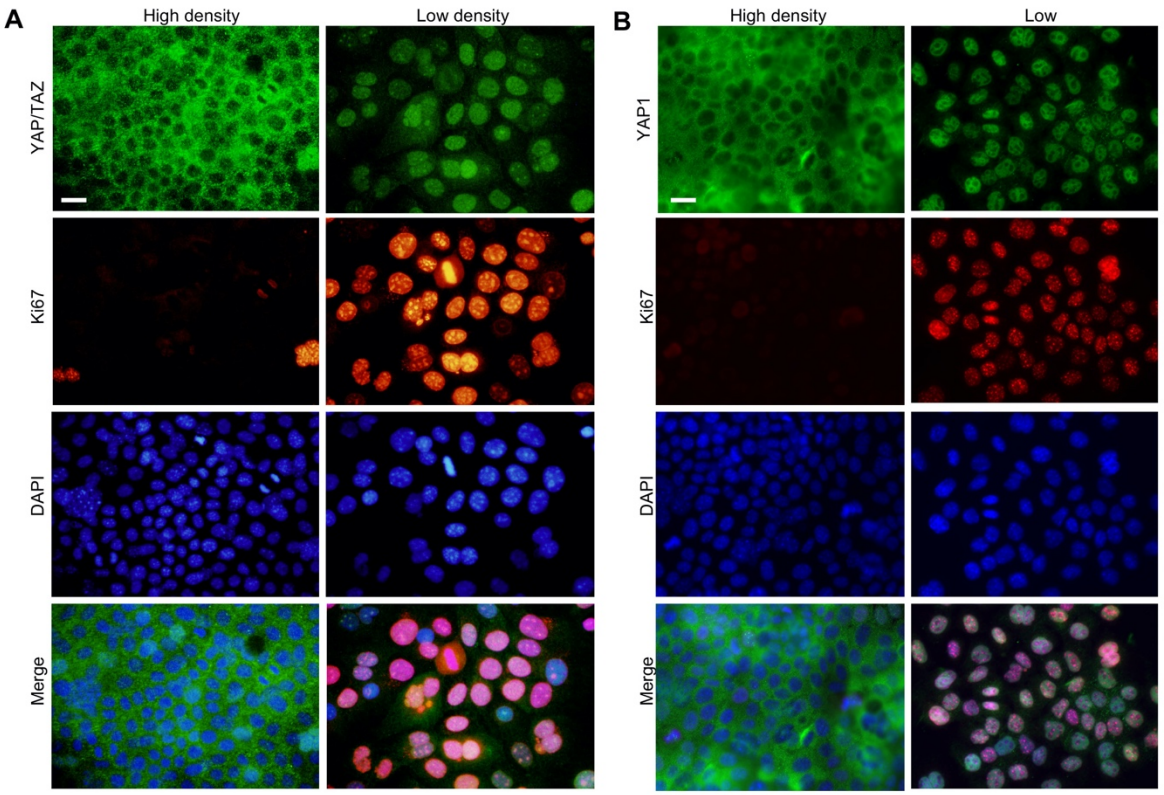

Figure S4. Cell-density-dependent expression of YAP/TAZ and ki67 in mHAT9d cells.

Immunostaining of YAP/TAZ and Ki67 (A), and YAP1 and Ki67 (B) in high-density (left) and low-density (right) mHAT9d cells under normoxia (21% O_2). Scale bars: 20 μm.

Supplementary Fig.5

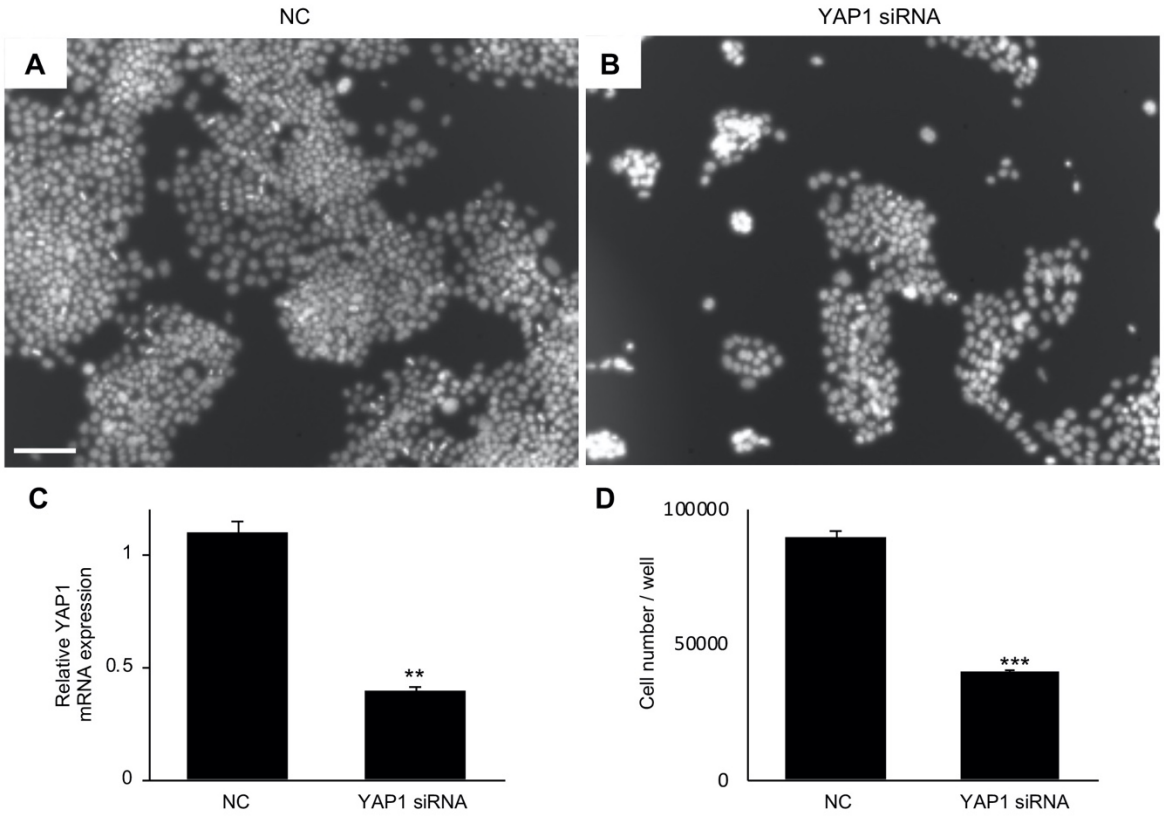

Figure S5. Effect of knocking down YAP1 expression on cell proliferation in mHAT9d cells. (A-B) DAPI staining of low-density mHAT9d cells transfected with non-specific control siRNA (NC) or siRNA specific for YAP1. (C) Expression of YAP1 mRNA in mHAT9d cells transfected with NC or siRNA specific for YAP1; n = 3. Data are represented as mean ± SEM. (D) The cells were counted 3 days after YAP1 siRNA transfection; n = 3. Data are represented as mean ± SEM. Scale bars: 100 μm.

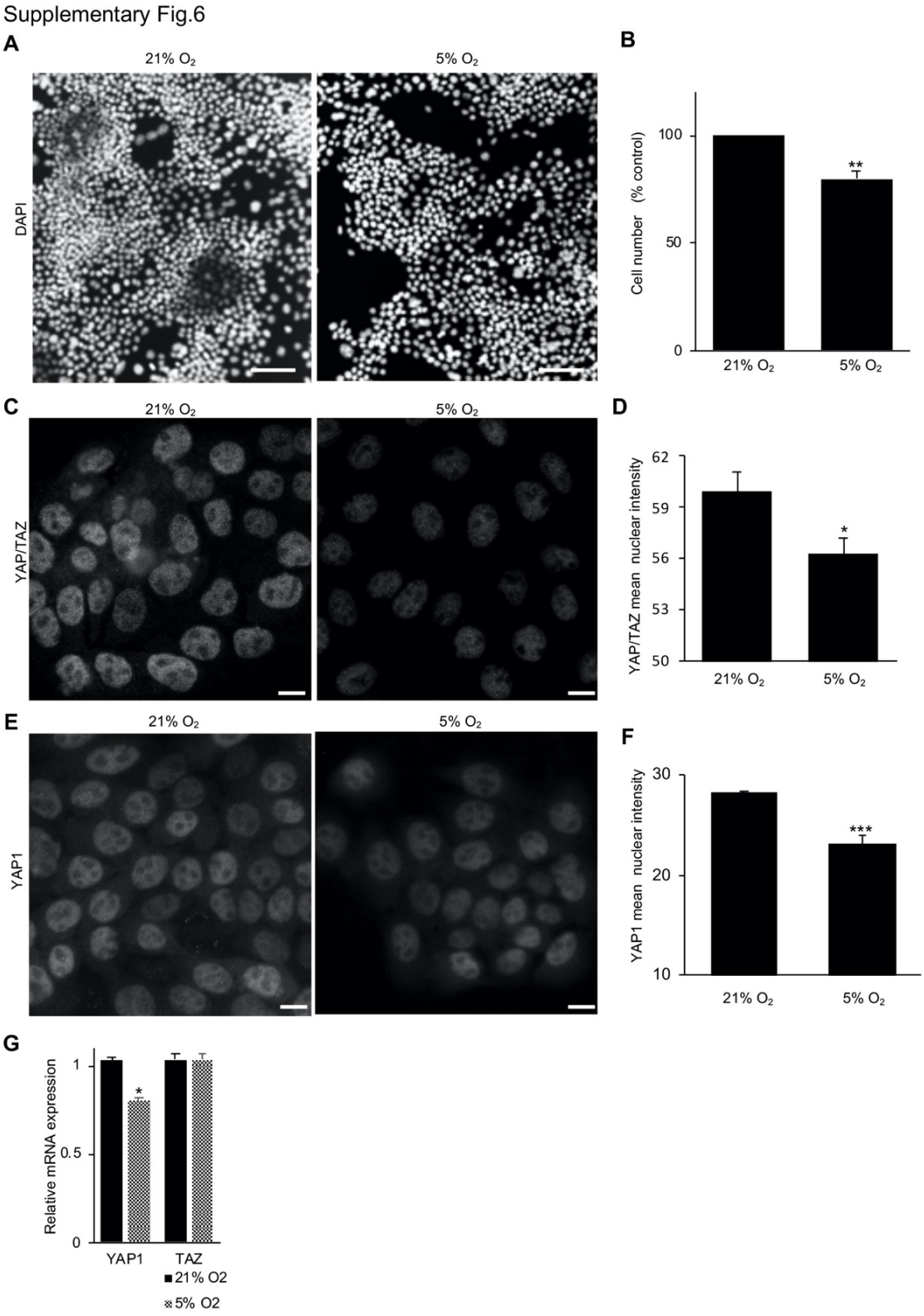

Figure S6. Effect of hypoxia on cell proliferation and YAP/TAZ expression in mHAT9d cells.

(A) DAPI staining of low-density mHAT9d cells cultured in normoxia (left) and hypoxia (right) for 3 days. (B) Quantification of cell number; n=4. Data are represented as mean ± SEM. (C) Immunostaining of YAP/TAZ in normoxia (left) and hypoxia (right) for 3 days. (D) Quantification of the intensity of nuclear YAP/TAZ fluorescence; n=4. (E) Immunostaining of YAP1 in normoxia (left) and hypoxia (right) for 3 days. (F) Quantification of the nuclear YAP1 fluorescence intensity; n = 4. (G) Expression of YAP1 and TAZ mRNA in mHAT9d cells cultured in normoxia and hypoxia; n = 4. Data are represented as mean ± SEM. Scale bars: (A) 100 μm; (C, E) 20 μm.

Supplementary Fig.7

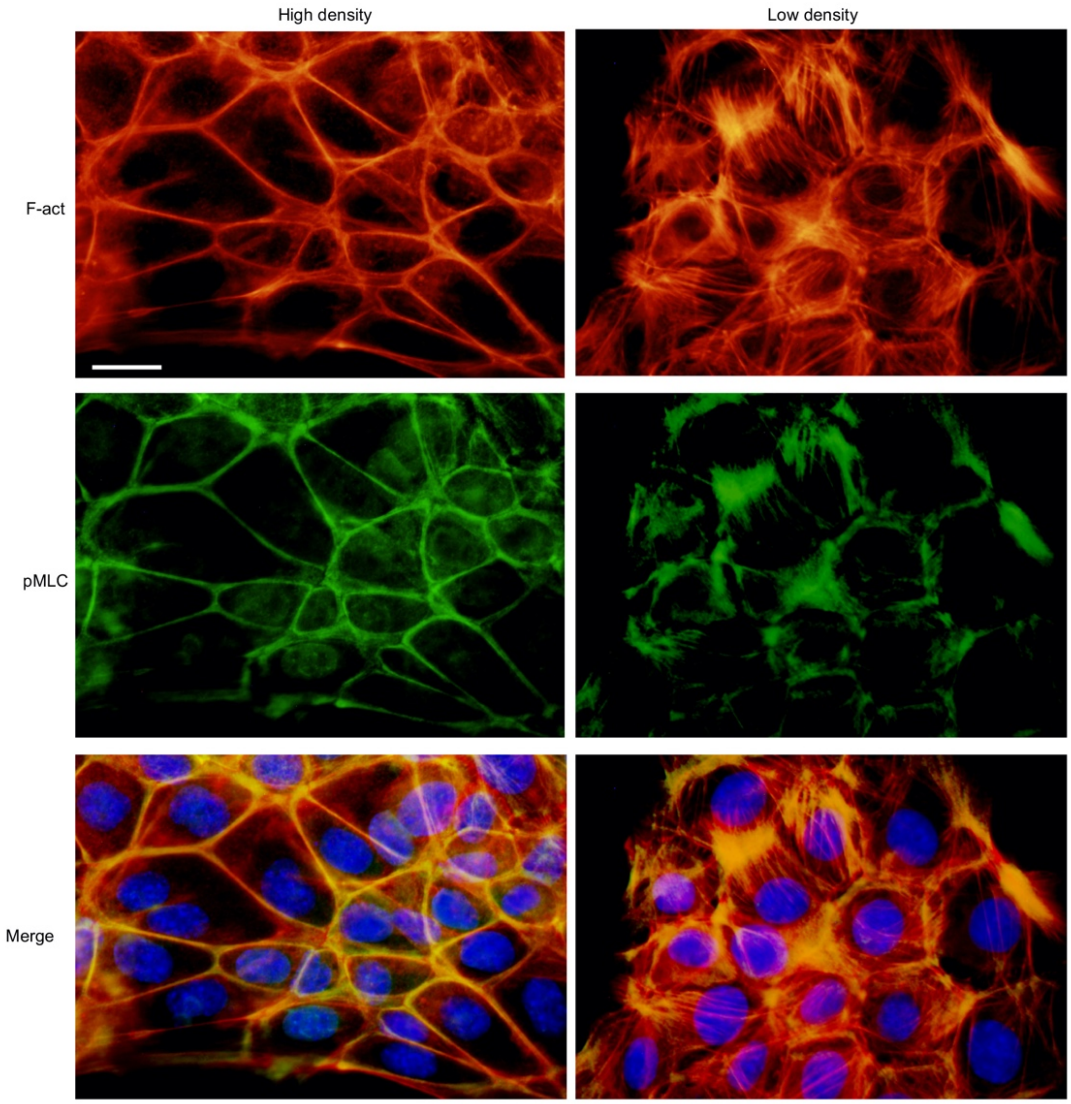

Figure S7. Cell-density-dependent expression of F-actin and pMLC in mHAT9d cells.

Phalloidin staining (F-actin) and immunostaining for pMLC in high-density (left) and low-density (right) mHAT9d cells under normoxia (21% O_2). Scale bars: 20 μm.

Supplementary Fig.8

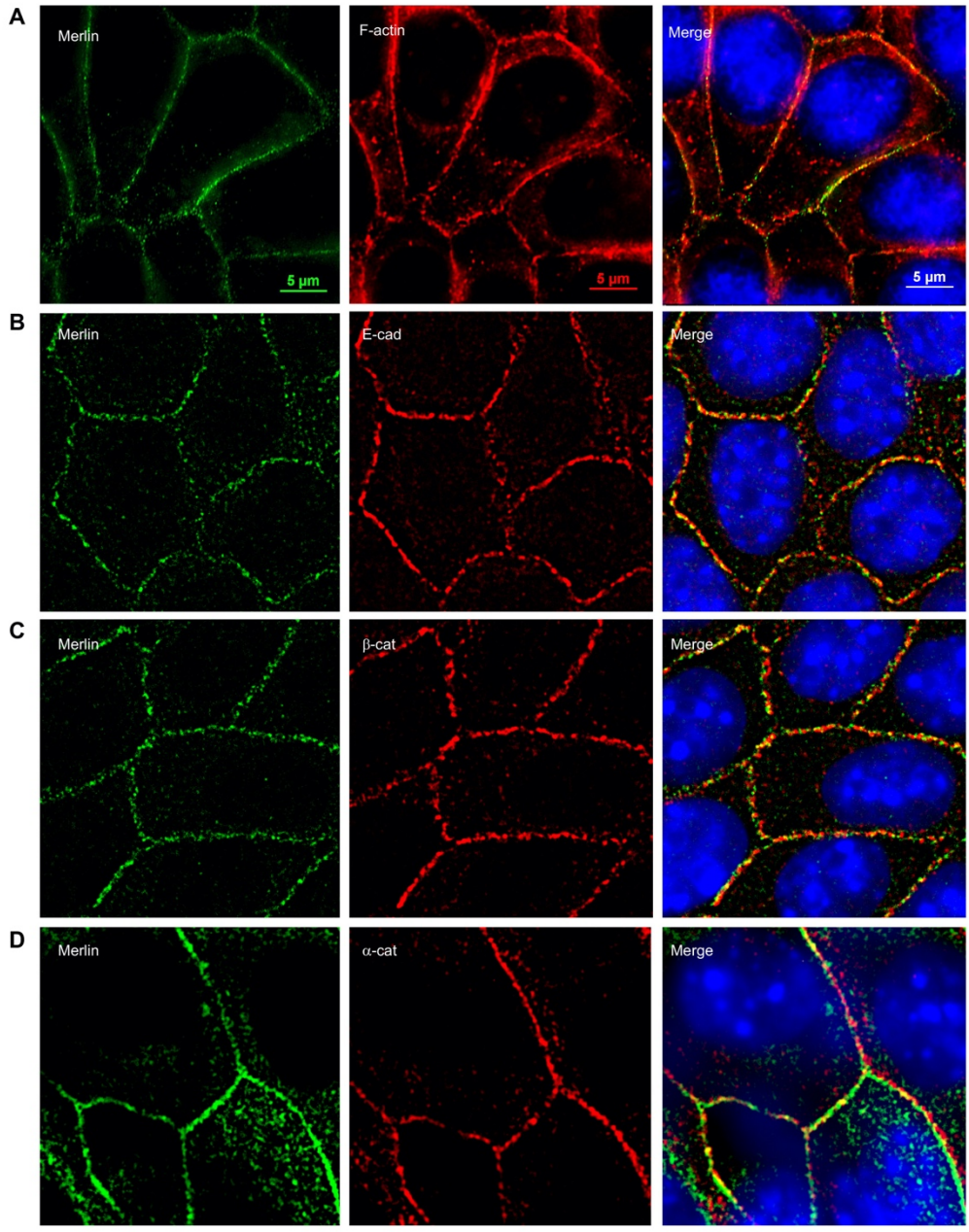

Figure S8. Co-expression of AJ protein in mHAT9d cells.

Images show the double staining for Merlin with F-actin (A), E-cadherin (B), β-catenin (C), and α-catenin (D) of high-density mHAT9d cells. Scale bars: 5 μm.

Supplementary Fig.9

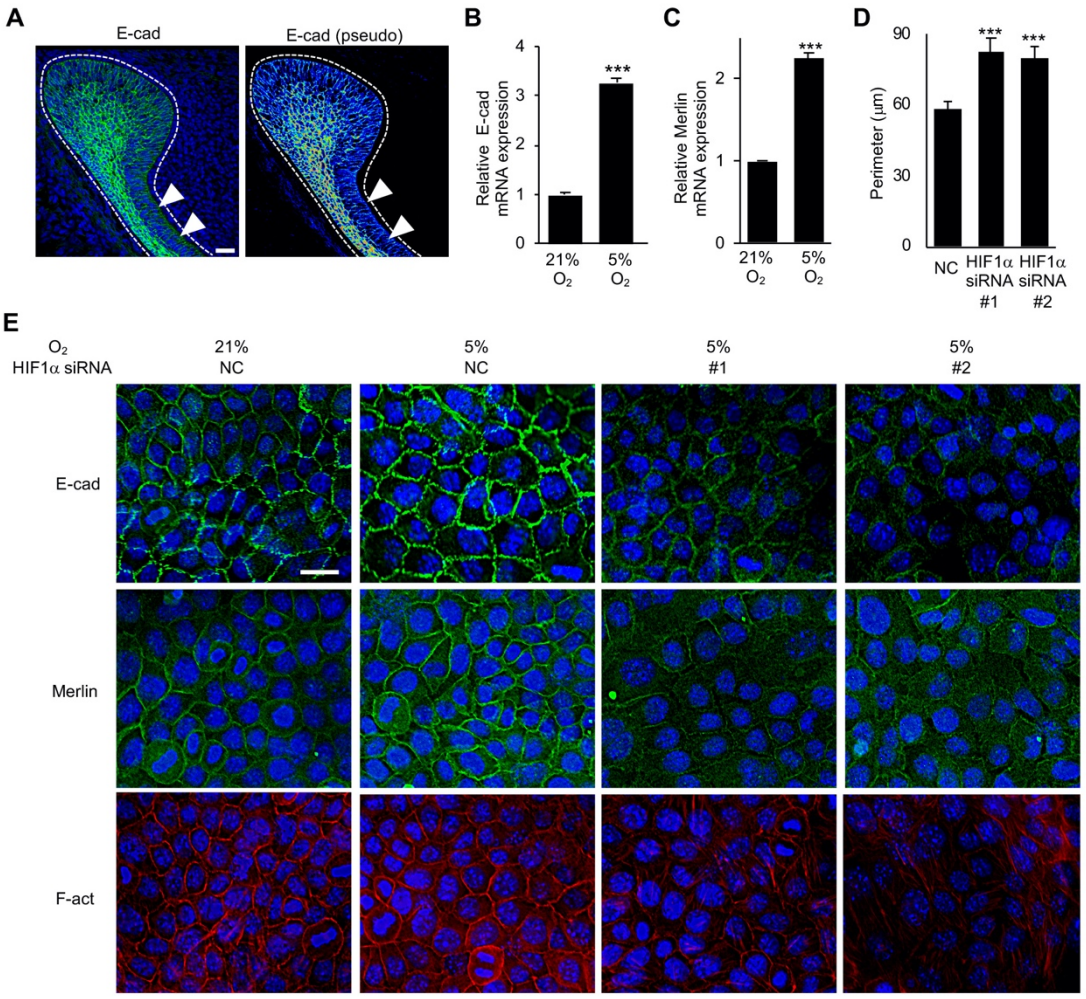

Figure S9. Effect of hypoxic signal on AJ proteins.

(A) Immunostaining of E-cadherin (E-cad) in a P3 mouse apical bud. (B, C) Expression of E-cadherin and Merlin mRNA in mHAT9d cells cultured in normoxia (21% 0_2) and hypoxia (5% O_2) for 1 day; n=3. Data are represented as mean ± SEM. (D) Average perimeter quantification of mHAT9d cells transfected with non-specific control siRNA (NC) or two different siRNA specific for HIF1α in hypoxia; n = 3. Data are represented as mean ± SEM. (E) Immunostaining of E-cadherin, Merlin, and Phalloidin staining (F-act) of high-density mHAT9d cells transfected with HIF1α siRNA in normoxia and hypoxia. Scale bars: (A) 30 μm; (E) 20 μm.